Chapter 13 Sub-Region Mixed Element Ⅱ—V-Notch Problem

Yu-Qiu Long
Department of Civil Engineering, School of Civil Engineering,
Tsinghua University, Beijing, 100084, China

Song Cen
Department of Engineering Mechanics, School of Aerospace,
Tsinghua University, Beijing, 100084, China

Abstract This chapter continues discussing the sub-region mixed element method. Here, the applications of the sub-region mixed element method in the analysis of the V-notches in plane problem, bi-material problem, Reissner plate problem, and 3D elastic body problem are focused on and discussed in turn. It is demonstrated again that the proposed sub-region mixed element method is efficient for such singular stress problems.

Keywords finite element, sub-region mixed element, V-notch problem.

13.1 Introduction

This chapter will discuss some topics about the stress analysis of structures with V-notches and the applications of the sub-region mixed element method.

Stress concentration will happen around the notches in structures, i.e., the stress fields at the tip of the notches possess singularity. Angular corners of holes and welding structures are all examples of the V-notch problem. An ideal straight crack can also be regarded as a V-notch with zero opening angle.

In this chapter, the sub-region mixed element analysis of the V-notches in plane problem[1], bi-material problem[2], Reissner plate problem[3] and 3D elastic body problem[4] will be discussed in turn.

13.2 Plane V-Notch Problem

Plane V-notch problems have always attracted much attention. In 1952, Williams[5] first established the eigenequations for the V-notch problem. He pointed out that

the stress at the notch-tip possesses singularity, and concluded that such singularity depends on the opening angle of the notch. Gross et al.[6] extended the concept of the stress intensity factors from ideal cracks into V-notch cases and evaluated the notch-tip stress intensity factors using a boundary collocation method. The boundary integral method has also been applied in reference [7] for the beam bending problem with a V-notch. The reciprocal work contour integral method was extended by Carpenter[8–10] into the analysis of stress concentration at the notch. Lin and Tong[11] proposed a hybrid singular element for the analysis of the V-notch problem. Awaji et al.[12] investigated the V-notches using dense triangular elements.

In this section, the sub-region mixed element method will be used for the analysis of the plane V-notch problem[1]. Firstly, by starting with the complex potentials of elasticity, the eigenproblem of the V-notch is discussed, and the variation regularity of the eigenvalue with the opening angle is given, in which the embranchment phenomenon of the high-order eigenvalue curve and the concept of the critical angle are also pointed out. Then, the expressions of the stress fields for modes Ⅰ and Ⅱ problems are given. Finally, the sub-region mixed element method is used to analyze the V-notch problem, which gives the results of the stress intensity factors K_{I} and K_{II} of the specimens containing V-notches with various angles.

13.2.1 Eigenproblem of V-Notches

The configuration of the elastic plane with a V-notch is shown in Fig. 13.1, the polar coordinate system is set. The stresses can be expressed in terms of two complex potentials $\phi(z)$ and $\psi(z)$ as follows:

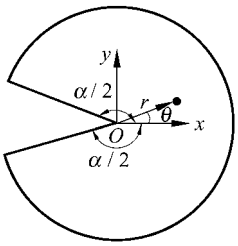

Figure 13.1 Stress analysis around a V-notch tip

$$\sigma_r + \sigma_\theta = 4\,\mathrm{Re}\,\phi'(z) \tag{13-1}$$

$$\sigma_\theta - \mathrm{i}\,\tau_{r\theta} = \phi'(z) + \overline{\phi'(z)} + \overline{z}\,\overline{\phi''(z)} + \overline{z}z^{-1}\overline{\psi'(z)} \tag{13-2}$$

The complex potentials can be expanded in series further

$$\left.\begin{aligned}\phi(x)&=\sum_{n=1}^{\infty}\frac{1}{2}(A_n z^{\lambda_n}+B_n z^{\bar{\lambda}_n})\\ \psi(x)&=\sum_{n=1}^{\infty}\frac{1}{2}(C_n z^{\lambda_n}+D_n z^{\bar{\lambda}_n})\end{aligned}\right\} \tag{13-3}$$

The stress boundary conditions for two unloaded surfaces of a V-notch are

$$(\sigma_\theta - \mathrm{i}\tau_{r\theta})\big|_{\theta=\pm\frac{\alpha}{2}}=0 \tag{13-4}$$

Then, from the above equations, we obtain

$$\left.\begin{aligned}C_n&=-A_n\lambda_n\cos\alpha-\bar{B}_n\cos\lambda_n\alpha\\ \bar{D}_n&=-A_n\cos\lambda_n\alpha-\bar{B}_n\lambda_n\cos\alpha\end{aligned}\right\} \tag{13-5}$$

$$\left.\begin{aligned}A_n\sin\lambda_n\alpha+\bar{B}_n\lambda_n\sin\alpha&=0\\ A_n\lambda_n\sin\alpha+\bar{B}_n\sin\lambda_n\alpha&=0\end{aligned}\right\} \tag{13-6}$$

Since stresses exist in the neighborhood of the notch-tip, the determinant of the coefficient matrix must be zero. Hence, two eigenequations can be obtained

$$\lambda_n\sin\alpha+\sin\lambda_n\alpha=0 \quad \text{(mode Ⅰ- symmetry)} \tag{13-7}$$

$$\lambda_n^*\sin\alpha-\sin\lambda_n^*\alpha=0 \quad \text{(mode Ⅱ- antisymmetry)} \tag{13-8}$$

From these eigenequations, two series of eigenvalues can be solved

$$\lambda_n=\xi_n+\mathrm{i}\eta_n,\quad \lambda_n^*=\xi_n^*+\mathrm{i}\eta_n^* \tag{13-9}$$

The eigenvalues λ_n and λ_n^* for α ranging from π to 2π are listed in Tables 13.1 and 13.2, respectively. And, a series of real part curves ξ_n-α (or ξ_n^*-α) and imaginary part curves η_n-α (or η_n^*-α) are also given in Figs. 13.2 and 13.3.

From these tables and figures, the following four points should be mentioned:

(1) The 3 eigenvalues ($\lambda=0$, $\lambda^*=0$, $\lambda^*=1$) are corresponding to the 3 states of rigid-body motion, so they should not be considered in practical analysis.

(2) The first eigenvalue λ_1 (or λ_1^*) is identical to a real number. The imaginary part curves η_1-α and η_1^*-α coincide with the abscissa axis. And, the real part curves ξ_1-α and ξ_1^*-α are smooth curves when $\pi\leqslant\alpha\leqslant 2\pi$. For the mode Ⅰ problem, the relation $0.5\leqslant\lambda_1<1$ is satisfied when the notch-tip angle α is in the range [π, 2π], hence, the stress singularity always exists in the notch-tip. For the mode Ⅱ problem, the relation $0.5\leqslant\lambda_1^*<1$ will not be satisfied unless the notch-tip angle α is in the range [4.493 409, 2π], thus, the stress singularity at the notch-tip does not always exist. In reference [11], the authors said that the mode Ⅱ

Table 13.1 Eigenvalues $\lambda_n = \xi_n \pm \mathrm{i}\eta_n$ for Mode Ⅰ (symmetry) problem

α	2π (360°)	6.108 652 (350°)	5.934 119 (340°)	5.855 023 (335.47°)	5.759 587 (330°)	5.499 379 (315.07°)	5.235 988 (300°)	4.712 389 (270°)
λ_1	0.5	0.500 053	0.500 427		0.501 453		0.512 222	0.544 484
λ_2	1.0	1.058 843	1.125 407		1.202 157	1.404 750	1.471 028 ±0.141 853i	1.629 257 ±0.231 251i
λ_3	1.5	1.499 728	1.497 614		1.490 378			
λ_4	2.0	2.118 822	2.267 187	2.402 415	2.440 492 ±0.114 207i		2.567 762 ±0.284 901i	2.971 844 ±0.373 931i
λ_5	2.5	2.497 980	2.476 770					

α	4.188 790 (240°)	3.665 191 (210°)	3.625 739 (207.74°)	3.490 659 (200°)	3.383 923 (193.88°)	3.316 126 (190°)	π (180°)
λ_1	0.615 731	0.751 973		0.818 703		0.900 042	1.0
λ_2	1.833 550 ±0.252 260i	2.106 29 ±0.096 099i	2.130 670	2.018 265		2.001 797	2.0
λ_3				2.420 588		2.695 23	3.0
λ_4	3.343 717 ±0.414 037i	3.828 294 ±0.347 177i		4.025 002 ±0.243 015i	4.156 771	4.022 68	4.0
λ_5						4.468 954	5.0

Table 13.2 Eigenvalues $\lambda_n^* = \xi_n^* \pm \mathrm{i}\eta_n^*$ for Mode Ⅱ (antisymmetry) problem

α	2π (360°)	6.108 652 (350°)	5.934 119 (340°)	5.932 123 (339.89°)	5.759 587 (330°)	5.732 235 (328.43°)	5.235 988 (300°)	4.712 389 (270°)
λ_1^*	0.5	0.529 355	0.562 007		0.598 192		0.730 901	0.908 529
λ_2^*	1.5	1.588 609	1.692 250		1.838 934	1.902 246	2.074 826 ±0.229 426i	2.301 328 ±0.315 837i
λ_3^*	2.0	1.999 107	1.991 385		1.948 556			
λ_4^*	2.5	2.649 696	2.883 887	2.902 967	2.987 005 ±0.166 741i		3.279 767 ±0.326 690i	3.641 420 ±0.418 787i
λ_5^*	3.0	2.996 141	2.920 168					

α	4.493 409 (257.45°)	4.188 790 (240°)	3.665 191 (210°)	3.490 659 (200°)	3.463 416 (198.44°)	3.336 226 (191.15°)	3.316 126 (190°)	π (180°)
λ_1^*	1.0	1.148 913	1.485 81	1.630 47			1.798 929	2.0
λ_2^*		2.589 479 ±0.348 375i	2.967 836 ±0.261 186i	3.122 551 ±0.108 732i	3.148 372		3.007 832	3.0
λ_3^*							3.586 718	4.0
λ_4^*		4.096 928 ±0.464 641i	4.688 039 ±0.409 575i	4.926 987 ±0.319 811i		5.161 747	5.060 484	5.0
λ_5^*							5.327 916	6.0

problem always possesses stress singularity when $\pi < \alpha \leqslant 2\pi$. This does not seem to be correct.

(3) The higher-order eigenvalues λ_n and λ_n^* may be complex numbers. The features of the curves of the higher-order eigenvalues can be described in detail as follows:

① When $\pi \leqslant \alpha \leqslant 2\pi$, these curves, which are not smooth curves any more,

consist of 3-piecewise curves, in which the middle segment and the two end segments are corresponding to complex roots and real roots, respectively. The positions of two conjunction points of 3-piecewise curves are corresponding to critical angles, α_{cr1} and α_{cr2}.

② The higher-order eigenvalues exist in pairs, for instance, λ_2 and λ_3 are a pair; λ_4 and λ_5 are a pair, etc. In addition, the curves of each pair of eigenvalues coincide in some ranges and then separate in other ranges. The real part curves ξ-α and ξ^*-α (see Figs. 13.2(a) and 13.3(a)) are separate curves in the two end ranges, and then coincide in the middle range. For example, the curves for ξ_2 and

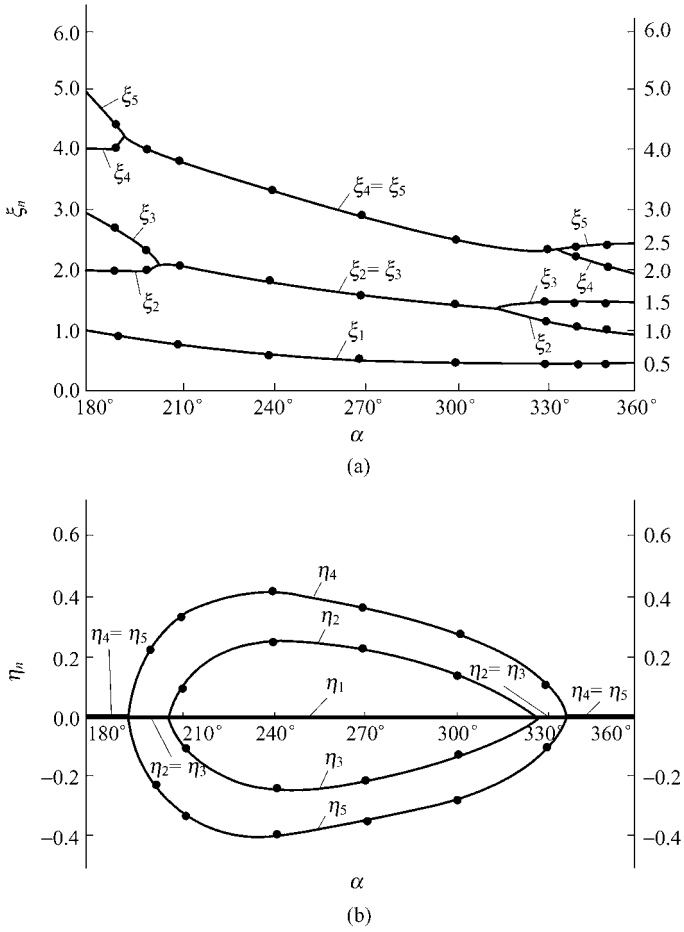

Figure 13.2 Real part and imaginary part curves of eigenvalues for Mode Ⅰ (symmetry) problem

(a) ξ_n-α curve; (b) η_n-α curve

ξ_3, which are two-branch curves in the two end ranges, will become a one-branch curve in the middle range after meeting at the critical angles α_{cr1} and α_{cr2}. Conversely, the imaginary part curves η-α and η^*-α (see Figs. 13.2(b) and 13.3(b)) are separated curves in the middle range, but will coincide in the two end ranges. For example, η_2 and η_3 are two symmetric curves (λ_2 and λ_3 are conjugate with each other) on the two sides of the abscissa axis in the middle range (complex root region), and will be merged into the abscissa axis in the two end ranges (real root regions).

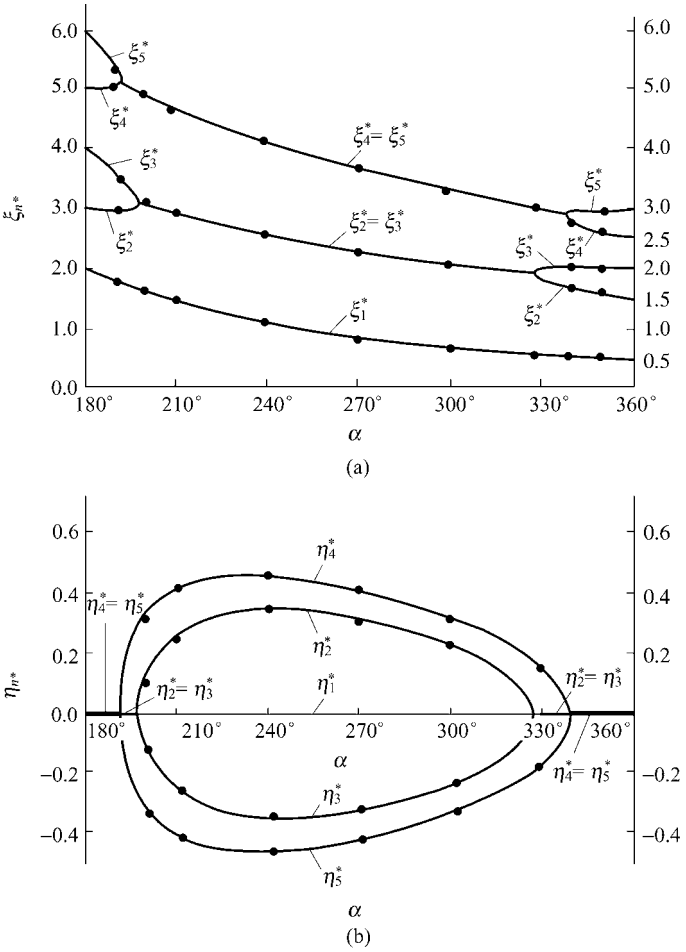

Figure 13.3 Real part and imaginary part curves of eigenvalues for Mode Ⅱ (antisymmetry) problem

(a) ξ_n^*-α curve; (b) η_n^*-α curve

The above features of the curves of the higher-order eigenvalues, such as appearance in pairs and the phenomenon of embranchment, have not been recognized by some authors in the early time. For example, the ξ-α curve in reference [8] does not reflect the characteristic of embranchment.

(4) For a certain notch-angle α, its eigenvalue series $\boldsymbol{\lambda}$ and $\boldsymbol{\lambda}^*$ are formed in the following manner: in the first place there are a few real roots in odd number, then followed by a sequence of conjugate complex roots in pairs. The number of real roots varies according to the notch-angle α. For $207.74^\circ<\alpha<315.07^\circ$, only one real root λ_1 exists among $\boldsymbol{\lambda}$. For $198.44^\circ<\alpha<328.43^\circ$, only one real root λ_1^* exists among $\boldsymbol{\lambda}^*$. The number of real roots will increase while α tends to π or 2π. When $\alpha=\pi$ or $\alpha=2\pi$, only real roots exist.

13.2.2 Stress Fields of the Mode Ⅰ (Symmetry) Problem

1. For complex eigenvalue λ_n

Substitution of Eq. (13-7) into Eqs. (13-6) and (13-5) yields

$$\bar{B}_n = A_n, \quad C_n = \bar{D}_n = -A_n(\lambda_n \cos\alpha + \cos\lambda_n\alpha) \tag{13-10}$$

The stresses pertaining to the complex eigenvalue λ_n for mode Ⅰ problem are

$$\boldsymbol{\sigma}_n = \begin{Bmatrix} \sigma_{r,n} \\ \sigma_{\theta,n} \\ \sigma_{r\theta,n} \end{Bmatrix} = \begin{bmatrix} \mathrm{Re}\,J_n & \mathrm{Im}\,J_n \\ \mathrm{Re}\,G_n & \mathrm{Im}\,G_n \\ \mathrm{Re}\,H_n & \mathrm{Im}\,H_n \end{bmatrix} \begin{Bmatrix} \mathrm{Re}\,A_n \\ -\mathrm{Im}\,A_n \end{Bmatrix} \tag{13-11}$$

where

$$\left.\begin{aligned} J_n &= r^{\lambda_n-1}\lambda_n[(3-\lambda_n)\cos(\lambda_n-1)\theta + (\lambda_n\cos\alpha+\cos\lambda_n\alpha)\cos(\lambda_n+1)\theta] \\ G_n &= r^{\lambda_n-1}\lambda_n[(\lambda_n+1)\cos(\lambda_n-1)\theta - (\lambda_n\cos\alpha+\cos\lambda_n\alpha)\cos(\lambda_n+1)\theta] \\ H_n &= r^{\lambda_n-1}\lambda_n[(\lambda_n-1)\sin(\lambda_n-1)\theta - (\lambda_n\cos\alpha+\cos\lambda_n\alpha)\sin(\lambda_n+1)\theta] \end{aligned}\right\} \tag{13-12}$$

The eigenroots are pairs of conjugate complex number. Let λ_n and λ_{n+1} be a pair of conjugate complex roots, we have

$$J_{n+1} = \bar{J}_n, \quad G_{n+1} = \bar{G}_n, \quad H_{n+1} = \bar{H}_n \tag{13-13}$$

Therefore, the stresses pertaining to this pair of conjugate complex roots can be written as

$$\boldsymbol{\sigma}_n + \boldsymbol{\sigma}_{n+1} = \begin{bmatrix} \mathrm{Re}\,J_n & \mathrm{Im}\,J_n \\ \mathrm{Re}\,G_n & \mathrm{Im}\,G_n \\ \mathrm{Re}\,H_n & \mathrm{Im}\,H_n \end{bmatrix} \begin{Bmatrix} \beta_n \\ \beta_{n+1} \end{Bmatrix} \tag{13-14}$$

in which two undetermined stress parameters β_n and β_{n+1} are included.

2. For real eigenvalue λ_n

When λ_n is real, J_n, G_n and H_n in Eq. (13-12) are all real numbers. So, Eq. (13-11) will degenerate into

$$\boldsymbol{\sigma}_n = \begin{Bmatrix} J_n \\ G_n \\ H_n \end{Bmatrix} \beta_n \tag{13-15}$$

in which only one undetermined stress parameter β_n is involved.

3. Mode Ⅰ stress intensity factor K_{I}

$$K_{\mathrm{I}} = \sqrt{2\pi} \lim_{r\to 0} r^{1-\lambda_1}\, \sigma_{\theta,1}\big|_{\theta=0} = \sqrt{2\pi}\beta_1\lambda_1(\lambda_1 + 1 - \lambda_1\cos\alpha - \cos\lambda_1\alpha) \tag{13-16}$$

13.2.3 Stress Fields of the Mode Ⅱ (Antisymmetry) Problem

1. For complex eigenvalue λ_n^*

Substitution of Eq. (13-8) into Eqs. (13-6) and (13-5) yields

$$\bar{B}_n^* = -A_n^*, \quad C_n^* = -\bar{D}_n^* = -A_n^*(\lambda_n^*\cos\alpha - \cos\lambda_n^*\alpha) \tag{13-17}$$

The stresses pertaining to the complex eigenvalue λ_n^* for mode Ⅱ problem are

$$\boldsymbol{\sigma}_n = \begin{bmatrix} \mathrm{Re}\,J_n^* & \mathrm{Im}\,J_n^* \\ \mathrm{Re}\,G_n^* & \mathrm{Im}\,G_n^* \\ \mathrm{Re}\,H_n^* & \mathrm{Im}\,H_n^* \end{bmatrix} \begin{Bmatrix} \mathrm{Im}\,A_n^* \\ \mathrm{Re}\,A_n^* \end{Bmatrix} \tag{13-18}$$

where

$$\left.\begin{aligned} J_n^* &= -r^{\lambda_n^*-1}\lambda_n^*[(3-\lambda_n^*)\sin(\lambda_n^*-1)\theta + (\lambda_n^*\cos\alpha - \cos\lambda_n^*\alpha)\sin(\lambda_n^*+1)\theta] \\ G_n^* &= -r^{\lambda_n^*-1}\lambda_n^*[(\lambda_n^*+1)\sin(\lambda_n^*-1)\theta - (\lambda_n^*\cos\alpha - \cos\lambda_n^*\alpha)\sin(\lambda_n^*+1)\theta] \\ H_n^* &= -r^{\lambda_n^*-1}\lambda_n^*[(1-\lambda_n^*)\cos(\lambda_n^*-1)\theta + (\lambda_n^*\cos\alpha - \cos\lambda_n^*\alpha)\cos(\lambda_n^*+1)\theta] \end{aligned}\right\} \tag{13-19}$$

The stresses pertaining to the conjugate complex roots λ_n^* and λ_{n+1}^* can be written as

$$\boldsymbol{\sigma}_n + \boldsymbol{\sigma}_{n+1} = \begin{bmatrix} \mathrm{Re}\, J_n^* & \mathrm{Im}\, J_n^* \\ \mathrm{Re}\, G_n^* & \mathrm{Im}\, G_n^* \\ \mathrm{Re}\, H_n^* & \mathrm{Im}\, H_n^* \end{bmatrix} \begin{Bmatrix} \beta_n^* \\ \beta_{n+1}^* \end{Bmatrix} \tag{13-20}$$

2. For real eigenvalue λ_n^*

$$\boldsymbol{\sigma}_n = \begin{Bmatrix} J_n^* \\ G_n^* \\ H_n^* \end{Bmatrix} \beta_n^* \tag{13-21}$$

3. Mode Ⅱ stress intensity factor K_{II}

$$K_{\mathrm{II}} = \sqrt{2\pi} \lim_{r\to 0} r^{1-\lambda_1^*} \tau_{r\theta,1}\big|_{\theta=0} = \sqrt{2\pi}\beta_1^*(-\lambda_1^*)(1-\lambda_1^* + \lambda_1^* \cos\alpha - \cos\lambda_1^*\alpha) \tag{13-22}$$

13.2.4 The Sub-Region Mixed Element Method

Now, the plane V-notch problem is considered using the sub-region mixed element method. The sectorial region of radius *R*, centered on the notch-tip is regarded as the complementary energy region (C-region), and the outside domain as the potential energy region (P-region). And, the P-region is modelled by the 8-node displacement-based isoparametric elements (see Fig. 13.4).

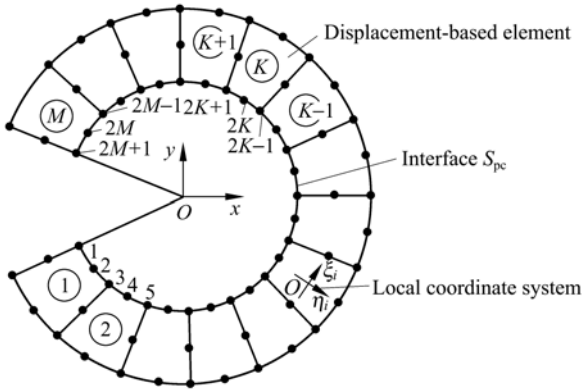

Figure 13.4 Stress-based element and outside 8-node isoparametric elements

The energy functional of the sub-region mixed variational principle is still given by Eq. (12-13), in which the matrices $\boldsymbol{F}$ and $\boldsymbol{H}$ can be derived as follows.

(1) The flexibility matrix $\boldsymbol{F}$ of the C-region

The stress fields of the C-region for modes Ⅰ and Ⅱ have already been derived, respectively. Here, the stress fields can be expressed in terms of the stress parameters $\boldsymbol{\beta}$ as

$$\boldsymbol{\sigma} = [\sigma_r \quad \sigma_\theta \quad \tau_{r\theta}]^{\mathrm{T}} = \boldsymbol{S}\boldsymbol{\beta} \tag{13-23}$$

Then, the complementary energy Π_{c} of the C-region and its flexibility matrix $\boldsymbol{F}$ can be written as

$$\begin{aligned} \Pi_{\mathrm{c}} &= \frac{1}{2}\boldsymbol{\beta}^{\mathrm{T}}\boldsymbol{F}\boldsymbol{\beta} \\ \boldsymbol{F} &= \int_{A_{\mathrm{c}}} \boldsymbol{S}^{\mathrm{T}}\boldsymbol{D}^{-1}\boldsymbol{S}h\mathrm{d}A \end{aligned} \tag{13-24}$$

where $\boldsymbol{D}$ is the elastic coefficient matrix; $\boldsymbol{D}^{-1}$ is given by Eq. (12-32). h is the thickness; and A_{c} is the area of the sectorial region in the C-region.

(2) The mixed matrix $\boldsymbol{H}$ on the interface

The mixed matrix $\boldsymbol{H}$ on the interface is still given by Eq. (12-45), i.e.,

$$\boldsymbol{H} = \int_{S_{\mathrm{pc}}} \boldsymbol{S}^{\mathrm{T}}\boldsymbol{L}^{\mathrm{T}}\bar{\boldsymbol{N}}h\mathrm{d}s \tag{13-25}$$

where $\boldsymbol{S}$ is defined by Eq. (13-23); $\boldsymbol{L}$ is the direction cosine matrix, and given by Eq. (12-41); $\bar{\boldsymbol{N}}$ is the shape function matrix of the 8-node isoparametric element. In Fig. 13.4, there are M isoparametric elements along the interface S_{pc}, then the components in matrix $\bar{\boldsymbol{N}}$ are

$$\left.\begin{aligned} \bar{N}_1 &= -\frac{1}{2}\xi_1(1-\xi_1) \\ \bar{N}_{2k} &= 1-\xi_k^2 \\ \bar{N}_{2k+1} &= \begin{cases} \dfrac{1}{2}\xi_k(1+\xi_k) & (\text{element } k) \\ -\dfrac{1}{2}\xi_{k+1}(1-\xi_{k+1}) & (\text{element } k+1) \end{cases} \\ \bar{N}_{2M+1} &= \frac{1}{2}\xi_M(1+\xi_M) \end{aligned}\right\} \begin{aligned} &(1 \leqslant k \leqslant M) \\ &(1 \leqslant k \leqslant M-1) \end{aligned} \tag{13-26}$$

h is the thickness (in Eq. (12-45), $h = 1$ is assumed).

(3) The stress intensity factors

Substitution of $\boldsymbol{F}$ and $\boldsymbol{H}$ obtained into Eq. (12-13) yields the expression of the energy functional Π. The basic unknowns $\boldsymbol{\delta}$ and $\boldsymbol{\beta}$ are still solved from the

stationary conditions (12-19) and (12-16). Finally, the stress intensity factors K_{I} and K_{II} can be obtained from Eqs. (13-16) and (13-22).

The sub-region mixed element method for the plane V-notch problem is denoted as SRM-V1.

Example 13.1 Evaluate the stress intensity factor K_{I} of a V-notched specimen subjected to uniform tension.

The geometry of the specimen is shown in Fig. 13.5(a), in which $\frac{H}{w}=1.0$; the Poisson's ratio $\mu=0.3$. Due to the symmetry, only half of the specimen is considered. Two meshes used here are shown in Figs. 13.5(b) and (c), which contain 11 and 22 elements, respectively.

The numerical results of the dimensionless stress intensity factor $K_{\mathrm{I}}/(\sigma w^{1-\lambda_1})$ for the various angles α are listed in Table 13.3 $\left(\text{assume } \frac{a}{w}=0.4\right)$. It can be seen that, in comparison with the results given by reference [6], the relative errors are all less than 0.6% for mesh Ⅱ.

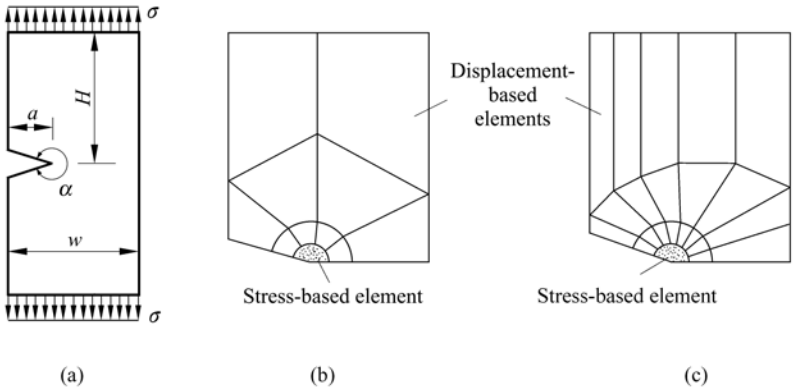

Figure 13.5 A V-notched specimen subjected to uniform tension
(a) Geometry; (b) Mesh Ⅰ; (c) Mesh Ⅱ

The results for various a/w are listed in Table 13.4 (assume $\alpha=300^\circ$). In comparison with the results given by reference [6], the relative errors are no larger than 0.6% for mesh Ⅱ.

Example 13.2 Evaluate the stress intensity factor K_{II} of a V-notched specimen subjected to antisymmetric load.

A single edge notched specimen is shown in Fig. 13.6(a): $a/w=0.333$, $H/a=1.0$, $\mu=0.3$. And, the mesh used for this example is shown in Fig. 13.6(b).

Table 13.3 $K_1/(\sigma w^{1-\lambda_1})$ for various α $\left(\frac{a}{w}=0.4\right)$

α	λ_1	Reference [6]	Mesh Ⅰ	Error (%)	Mesh Ⅱ	Error (%)
360°	0.500 000	2.369	2.314	−2.3	2.357	−0.5
350°	0.500 053	2.369	2.314	−2.3	2.357	−0.5
330°	0.501 453	2.389	2.313	−3.0	2.378	−0.5
300°	0.512 221	2.520	2.437	−3.3	2.514	−0.2
270°	0.544 484	2.888	2.795	−3.2	2.876	−0.4
240°	0.615 731	3.766	3.662	−2.8	3.754	−0.3

Table 13.4 $K_1/(\sigma w^{1-\lambda_1})$ for various a/w $(\alpha = 300°)$

a/w	Reference [6]	Mesh Ⅰ	Error (%)	Mesh Ⅱ	Error (%)
0.3	1.724	1.671	−3.1	1.713	−0.6
0.4	2.520	2.436	−3.3	2.511	−0.5
0.5	3.756	3.569	−5.0	3.736	−0.5
0.6	5.859	5.576	−4.8	5.761	−0.6

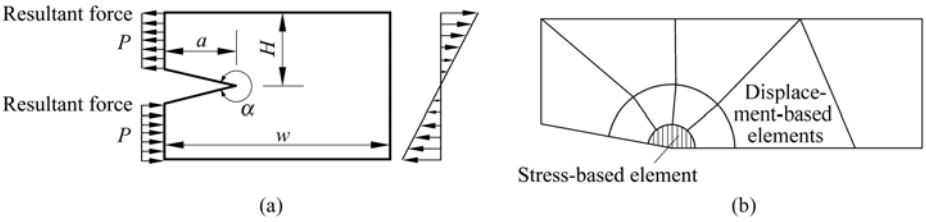

Figure 13.6 Single edge notched specimen subjected to antisymmetric load
(a) Geometry; (b) Mesh

For investigating the effect of the number of the eigenvalues considered on the stress intensity factors, the numerical results with which 1, 2, 3 and 4 eigenvalues are considered are given respectively in Table 13.5. It can be seen that satisfactory results can be obtained when the first 3 eigenvalues are used.

Table 13.5 $K_{II}(H/Pa^{1-\lambda_1^*})$ for various numbers of the first eigenvalues

α	λ_1^*	Number of eigenvalues considered				Reference [6]
		1	2	3	4	
360°	0.500 000	0.521	0.484	0.503	0.502	0.500
350°	0.529 355	0.425	0.388	0.405	0.404	0.401
340°	0.562 007	0.308	0.269	0.283	0.282	0.278

13.3 Plane V-Notch Problem in a Bi-Material

The plane V-notch problem in a bi-material not only keeps the main features of the plane V-notch problem for homogeneous material, but also reflects the characteristic of the interface crack. The singularities of stresses and strains at the notch-tip depend both on the opening angle of the notch and the ratio of the bi-material properties.

The plane V-notch problems in a bi-material have been discussed in references [2] and [13, 14]. In this section, the sub-region mixed element method will be used to analyze the V-notches in a bi-material[2]. Firstly, by starting with the potential function theory, the eigenequations for the plane V-notch problem in a bi-material are derived. Then, the eigenvalues are solved by Muller iteration method, and the displacement and stress fields around the notch-tip can be obtained. Finally, the stress intensity factors for the various opening angles and ratios of bi-material properties are solved by the sub-region mixed element method.

13.3.1 The Stress Fields Around the Notch-Tip

As shown in Fig. 13.7, the V-notch is composed of two kinds of materials. Their shear elastic moduli are G_1 and G_2, respectively; and the Poisson's ratios are μ_1 and μ_2.

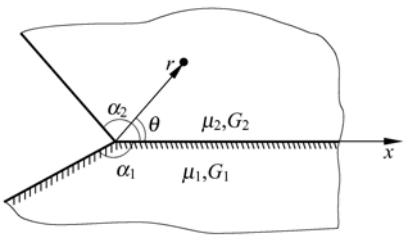

Figure 13.7 A V-notch in a bi-material

Let the notch-tip be the origin of the coordinate system, and the interface line be the x-axis. Then, the two sides of the notch are given by

$$\theta = -\alpha_1, \quad \theta = \alpha_2$$

Let $i = 1, 2$ denote material 1 and material 2, respectively. Then, the stress fields of this bi-material can be derived as follows.

(1) The stress functions φ_1 and φ_2

φ_1 and φ_2 denote the stress functions of material 1 and 2, respectively. In polar coordinates r and θ, they can be expressed in the following form of separated variables:

$$\varphi_i = r^{\lambda+1} f_i(\theta, \lambda) \quad (i = 1, 2) \tag{13-27}$$

where λ is the eigenvalue.

Since both the stress functions φ_1 and φ_2 should satisfy the bi-harmonic equation, f_i in the above equation should be

$$f_i = a_i \sin(\lambda+1)\theta + b_i \cos(\lambda+1)\theta + c_i \sin(\lambda-1)\theta + d_i \cos(\lambda-1)\theta \quad (i=1,2) \tag{13-28}$$

Thus, the stresses and displacements of the bi-material can be expressed in terms of f_i as follows

$$\left.\begin{aligned}
&\sigma_{irr} = r^{\lambda-1}[f_i'' + (\lambda+1)f_i] \\
&\sigma_{i\theta\theta} = r^{\lambda-1}[\lambda(\lambda+1)f_i] \\
&\sigma_{ir\theta} = r^{\lambda-1}[-\lambda f_i'] \\
&u_{ir} = \frac{r^{\lambda}}{2G_i}\{-(\lambda+1)f_i + (\lambda\omega_i)^{-1}[f_i'' + (\lambda+1)^2 f_i]\} \\
&u_{i\theta} = \frac{r^{\lambda}}{2G_i}\{-f_i' - (\lambda(\lambda-1)\omega_i)^{-1}[f_i''' + (\lambda+1)^2 f_i']\}
\end{aligned}\right\} \quad (i=1,2) \tag{13-29}$$

where f_i' is the first-order derivative of f_i with respect to θ, the rest may be inferred by analogy; G_i is the shear modulus; ω_i can be expressed as

$$\omega_i = \begin{cases} 1+\mu_i & \text{plane stress state} \\ \dfrac{1}{1-\mu_i} & \text{plane strain state} \end{cases}$$

in which μ_i is the Poisson's ratio of material *i*.

(2) The boundary and continuity conditions

From Eq. (13-28), it can be seen that f_1 and f_2 each contain 4 unknown parameters. These 8 unknown parameters can be written as

$$\boldsymbol{g} = [a_1 \quad b_1 \quad c_1 \quad d_1 \quad a_2 \quad b_2 \quad c_2 \quad d_2]^{\mathrm{T}} \tag{13-30}$$

In order to solve these unknown parameters, the following 8 conditions

$$\left.\begin{aligned}
&\sigma_{1\theta\theta} = 0 \\
&\sigma_{1r\theta} = 0
\end{aligned}\right\} \quad (\theta = -\alpha_1)$$

$$\left.\begin{aligned}
&\sigma_{2\theta\theta} = 0 \\
&\sigma_{2r\theta} = 0
\end{aligned}\right\} \quad (\theta = \alpha_2) \tag{13-31}$$

$$\left.\begin{aligned}
&\sigma_{1\theta\theta} = \sigma_{2\theta\theta} \\
&\sigma_{1r\theta} = \sigma_{2r\theta} \\
&u_{1r} = u_{2r} \\
&u_{1\theta} = u_{2\theta}
\end{aligned}\right\} \quad (\theta = 0)$$

can be introduced.

Substitution of Eq. (13-29) into the above equation yields 8 homogeneous conditions about the unknown parameters $\boldsymbol{g}$ as follows:

$$-a_1 \sin(\lambda+1)\alpha_1 + b_1 \cos(\lambda+1)\alpha_1 - c_1 \sin(\lambda-1)\alpha_1 + d_1 \cos(\lambda-1)\alpha_1 = 0 \tag{13-32a}$$

$$\begin{aligned} &a_1(\lambda+1)\cos(\lambda+1)\alpha_1 + b_1(\lambda+1)\sin(\lambda+1)\alpha_1 \\ &+ c_1(\lambda-1)\cos(\lambda-1)\alpha_1 + d_1(\lambda-1)\sin(\lambda-1)\alpha_1 = 0 \end{aligned} \tag{13-32b}$$

$$a_2 \sin(\lambda+1)\alpha_2 + b_2 \cos(\lambda+1)\alpha_2 + c_2 \sin(\lambda-1)\alpha_2 + d_2 \cos(\lambda-1)\alpha_2 = 0 \tag{13-32c}$$

$$\begin{aligned} &a_2(\lambda+1)\cos(\lambda+1)\alpha_2 - b_2(\lambda+1)\sin(\lambda+1)\alpha_2 \\ &+ c_2(\lambda-1)\cos(\lambda-1)\alpha_2 - d_2(\lambda-1)\sin(\lambda-1)\alpha_2 = 0 \end{aligned} \tag{13-32d}$$

$$b_1 + d_1 = b_2 + d_2 \tag{13-32e}$$

$$a_1(\lambda+1) + c_1(\lambda-1) = a_2(\lambda+1) + c_2(\lambda-1) \tag{13-32f}$$

$$\begin{aligned} &-(\lambda+1)(b_1+d_1) + (\lambda\omega_1)^{-1}[-b_1(\lambda+1)^2 - d_1(\lambda-1)^2 + (\lambda+1)(b_1+d_1)] \\ &= -(\lambda+1)(b_2+d_2) + (\lambda\omega_2)^{-1}[-b_2(\lambda+1)^2 - d_2(\lambda-1)^2 + (\lambda+1)(b_2+d_2)] \end{aligned} \tag{13-32g}$$

$$\begin{aligned} &-a_1(\lambda+1) - c_1(\lambda-1) - (\lambda(\lambda-1)\omega_1)^{-1}\{-a_1(\lambda+1)^3 \\ &-c_1(\lambda-1)^3 + (\lambda+1)^2[(\lambda+1)a_1 + (\lambda-1)c_1]\} \\ &= -a_2(\lambda+1) - c_2(\lambda-1) - (\lambda(\lambda-1)\omega_2)^{-1}\{-a_2(\lambda+1)^3 \\ &-c_2(\lambda-1)^3 + (\lambda+1)^2[(\lambda+1)a_2 + (\lambda-1)c_2]\} \end{aligned} \tag{13-32h}$$

The above 8 homogeneous equations can be rewritten in the following matrix form:

$$\boldsymbol{G}\boldsymbol{g} = \boldsymbol{0} \tag{13-33}$$

where the unknown parameters in $\boldsymbol{g}$ are defined by Eq. (13-30); and $\boldsymbol{G}$ is the coefficient matrix of the equation set (13-32).

(3) Eigenequaiton and the first n eigenvalues

In order to obtain the nonzero solutions of the homogeneous Eq. (13-33), let the determinant of the coefficient matrix $\boldsymbol{G}$ be zero:

$$|\boldsymbol{G}| = 0 \tag{13-34}$$

This is the eigenequaiton of the plane V-notch problem in a bi-material.

By using the Muller iteration method, a series of eigenvalues of the eigenequaiton (13-34) can be solved. The first n eigenvalues are written by

$$\boldsymbol{\lambda} = [\lambda_1 \quad \lambda_2 \quad \cdots \quad \lambda_n]^{\mathrm{T}} \tag{13-35}$$

(4) Stress expansion around the notch-tip

Substituting any eigenvalue λ_k in $\boldsymbol{\lambda}$ into Eq. (13-33), a set of nonzero solutions $\boldsymbol{g}_{(k)}$ of $\boldsymbol{g}$ can be obtained. We can only determine the ratio of each component to the first component a_{1k} in $\boldsymbol{g}_{(k)}$, but a_{1k} is still an unknown value. That is to say, each component in $\boldsymbol{g}_{(k)}$ can be expressed as a known multiple of a_{1k}. Substitution of $\boldsymbol{g}_{(k)}$ into Eq. (13-29) yields the stress terms corresponding to the eigenvalue λ_k:

$$\boldsymbol{\sigma}_{i(k)} = \begin{Bmatrix} \sigma_{irr} \\ \sigma_{i\theta\theta} \\ \sigma_{ir\theta} \end{Bmatrix}_{(k)} = \boldsymbol{J}_{i(k)} a_{1k} \quad (i = 1, 2) \tag{13-36}$$

By superposition of the stress terms corresponding to the first n eigenvalues, the stress expansion can be obtained as follows:

$$\boldsymbol{\sigma}_i = \begin{Bmatrix} \sigma_{irr} \\ \sigma_{i\theta\theta} \\ \sigma_{ir\theta} \end{Bmatrix} = \boldsymbol{S}_i \boldsymbol{\beta} \quad (i = 1, 2) \tag{13-37}$$

where

$$\left.\begin{aligned} \boldsymbol{\beta} &= [a_{11} \quad a_{12} \quad \cdots \quad a_{1n}]^{\mathrm{T}} \\ \boldsymbol{S}_i &= [\boldsymbol{J}_{i(1)} \quad \boldsymbol{J}_{i(2)} \quad \cdots \quad \boldsymbol{J}_{i(n)}] \end{aligned}\right\} \tag{13-38}$$

The unknown coefficients in $\boldsymbol{\beta}$ will be determined by the sub-region mixed element method.

13.3.2 The Sub-Region Mixed Element Method

Now, the sub-region mixed element method is used to analyze the plane V-notch problem in a bi-material. The sectorial region centered at the notch-tip is taken as the complementary energy region A_{c}, which is composed of two kinds of materials and denoted as A_{c1} and A_{c2}, respectively (Fig. 13.8). The outside of the C-region is the potential energy region A_{p}, which is composed of A_{p1} and A_{p2} and modelled by 8-node displacement-based isoparametric elements. And, the interface S_{pc} is composed of S_{pc1} and S_{pc2}.

The energy functional of the sub-region mixed variational principle is still given by Eq. (12-13), in which the matrices $\boldsymbol{F}$ and $\boldsymbol{H}$ can be derived as follows.

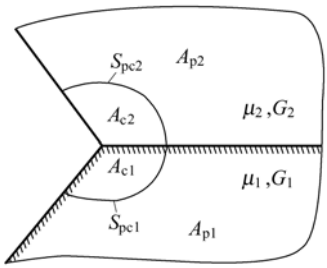

Figure 13.8 Division of the C-region and P-region
(V-notch in a bi-material)

(1) The flexibility matrix $\boldsymbol{F}$ of the C-region

The complementary energy Π_c of the C-region is

$$\Pi_c = \frac{1}{2}\iint_{A_{c1}} \boldsymbol{\sigma}_1^{\mathrm{T}} \boldsymbol{D}_1^{-1} \boldsymbol{\sigma}_1 h \mathrm{d}A + \frac{1}{2}\iint_{A_{c2}} \boldsymbol{\sigma}_2^{\mathrm{T}} \boldsymbol{D}_2^{-1} \boldsymbol{\sigma}_2 h \mathrm{d}A \tag{13-39}$$

in which stresses $\boldsymbol{\sigma}_i$ are expressed by Eq. (13-37), so we have

$$\Pi_c = \frac{1}{2}\boldsymbol{\beta}^{\mathrm{T}} \boldsymbol{F} \boldsymbol{\beta} \tag{13-40}$$

Then, the flexibility matrix $\boldsymbol{F}$ can be written as

$$\boldsymbol{F} = \iint_{A_{c1}} \boldsymbol{S}_1^{\mathrm{T}} \boldsymbol{D}_1^{-1} \boldsymbol{S}_1 h \mathrm{d}A + \iint_{A_{c2}} \boldsymbol{S}_2^{\mathrm{T}} \boldsymbol{D}_2^{-1} \boldsymbol{S}_2 h \mathrm{d}A \tag{13-41}$$

where $\boldsymbol{D}_1$ and $\boldsymbol{D}_2$ are the elastic matrices of the materials 1 and 2, respectively.

(2) The mixed matrix $\boldsymbol{H}$ on the interface

The additional energy H_{pc} on the interface is composed of two parts. According to Eq. (12-8), H_{pc} can be expressed as

$$H_{pc} = \int_{S_{pc1}} \boldsymbol{T}_1^{\mathrm{T}} \overline{\boldsymbol{u}}_1 h \mathrm{d}s + \int_{S_{pc2}} \boldsymbol{T}_2^{\mathrm{T}} \overline{\boldsymbol{u}}_2 h \mathrm{d}s \tag{13-42}$$

$\boldsymbol{T}_i$ is the boundary force of the C-region on the interface S_{pci}; $\overline{\boldsymbol{u}}_i$ is the boundary displacement of the P-region on the interface S_{pci}:

$$\left.\begin{aligned} \boldsymbol{T}_i &= \boldsymbol{L}_i \boldsymbol{\sigma}_i = \boldsymbol{L}_i \boldsymbol{S}_i \boldsymbol{\beta} \\ \overline{\boldsymbol{u}}_i &= \overline{\boldsymbol{N}}_i \overline{\boldsymbol{\delta}} \end{aligned}\right\} \tag{13-43}$$

where $\boldsymbol{L}_1$ and $\boldsymbol{L}_2$ are the direction cosine matrix of the interface; $\overline{\boldsymbol{N}}_1$ and $\overline{\boldsymbol{N}}_2$ are formed by the shape functions of the displacement-based elements; $\overline{\boldsymbol{\delta}}$ is the nodal displacement vector of the nodes on the interface. Substitution of Eq. (13-43) into Eq. (13-42) yields

$$H_{\mathrm{pc}} = \boldsymbol{\beta}^{\mathrm{T}} \boldsymbol{H} \bar{\boldsymbol{\delta}} \tag{13-44}$$

And, the mixed matrix $\boldsymbol{H}$ on the interface can be derived:

$$\boldsymbol{H} = \int_{S_{\mathrm{pc}1}} \boldsymbol{S}_1^{\mathrm{T}} \boldsymbol{L}_1 \bar{\boldsymbol{N}}_1 h \mathrm{d}s + \int_{S_{\mathrm{pc}2}} \boldsymbol{S}_2^{\mathrm{T}} \boldsymbol{L}_2 \bar{\boldsymbol{N}}_2 h \mathrm{d}s \tag{13-45}$$

(3) The stress intensity factors

Substituting $\boldsymbol{F}$ and $\boldsymbol{H}$, which have been obtained, into Eq. (12-13), the expression of the energy functional Π can be obtained. The basic unknowns $\boldsymbol{\delta}$ and $\boldsymbol{\beta}$ are still solved by the stationary conditions (12-19) and (12-16).

From $\boldsymbol{\beta}$, the stresses $\sigma_{\theta\theta}$ and $\sigma_{r\theta}$ can be determined. And, the stress intensity factor of the notch-tip can be determined from the following definition:

$$\left.\begin{aligned} K_{\mathrm{I}} &= \sqrt{2\pi} \lim_{r \to 0} r^{1-\lambda_1} \sigma_{\theta\theta}\big|_{\theta=0} \\ K_{\mathrm{II}} &= \sqrt{2\pi} \lim_{r \to 0} r^{1-\lambda_2} \sigma_{r\theta}\big|_{\theta=0} \end{aligned}\right\} \tag{13-46}$$

The sub-region mixed element method for the plane V-notch problem in a bi-material is denoted as SRM-V2.

Example 13.3 Evaluate the stress intensity factors K_{I} and K_{II} of a plate in extension with a V-notch at a bi-material interface by the sub-region mixed element method SRM-V2 (Fig. 13.9). The notch-tip is also at the bi-material interface.

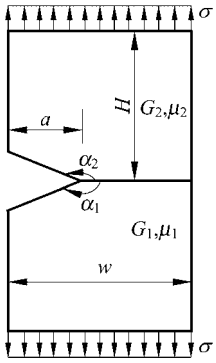

Figure 13.9 A plate in extension with a V-notch at a bi-material interface

Let $\mu_1 = \mu_2 = 0.3$; $H / w = 1.0$; and $\alpha_1 = \alpha_2$.

In order to check the effects on the stress intensity factors with the variations of different factors (ratios of material properties, opening angle of the notch and ratio of the notch length to plate width), the following two cases are considered:

(1) a/w ratio keeps invariant, but opening angles $\alpha_1 = \alpha_2$ of the notch and G_2 / G_1 ratio vary—Numerical results are listed in Table 13.6.

(2) Opening angles $\alpha_1 = \alpha_2$ keep invariant, but ratios of a / w and G_2 / G_1 vary—Numerical results are listed in Table 13.7.

From the above results, it can be concluded that

(1) For a symmetric notch subjected to symmetric load, the shear mode stress concentration phenomenon $(K_{II} \neq 0)$ will happen due to the difference of materials; when $G_2 / G_1 = 1,\ K_{II} = 0.$

Table 13.6 The stress intensity factors under various ratios of material properties and opening angles of the notch ($a / w = 0.4$)

$\alpha_1 = \alpha_2$	G_2/G_1	1			3	5	7	10
		SRM-V2	Reference[6]	Error (%)				
240°	$K_I / w^{1-\lambda_1}\sigma$	3.801	3.766	0.93	3.944	4.187	4.336	4.515
	$K_{II} / w^{1-\lambda_2}\sigma$	0.0	0.0		0.234	0.397	0.494	0.631
270°	$K_I / w^{1-\lambda_1}\sigma$	2.913	2.888	0.87	3.340	3.904	4.480	5.397
	$K_{II} / w^{1-\lambda_2}\sigma$	0.0	0.0		1.018	1.564	1.990	2.576

Table 13.7 Variations of the stress intensity factors with various ratios G_2 / G_1 and notch lengths ($\alpha_1 = \alpha_2 = 150^\circ$)

G_2 / G_1	a / w	0.3	0.4	0.5	0.6
1	$K_I / w^{1-\lambda_1}\sigma$	1.750	2.574	3.779	5.757
	$K_{II} / w^{1-\lambda_2}\sigma$	0.0	0.0	0.0	0.0
3	$K_I / w^{1-\lambda_1}\sigma$	2.400	3.428	4.988	7.554
	$K_{II} / w^{1-\lambda_2}\sigma$	1.278	1.717	2.398	3.541

(2) The singularity at the notch-tip will increase with the increase of the difference of materials.

(3) The singularity at the notch-tip will increase with the decrease of the opening angle of notch.

(4) The singularity at the notch-tip will increase with the increase of the notch length.

The first 4 eigenvalues are taken during the computations. If the radius of the singular element varies within the range $0.1a - 0.08a$, the results are relatively stable.

Example 13.4 Evaluate the stress intensity factors of a central crack at a bi-material interface in an infinite plate.

An infinite plate subjected to a uniform tension load $\sigma_y^{\infty} = 1\text{kPa}$ along y-direction is shown in Fig. 13.10. There is an interface crack with length $2a = 2\text{m}$ located at

the center of the bi-material interface. And, the Young's modulus $E_1 = 1\text{kPa}$; the Poisson's ratios $\mu_1 = \mu_2 = 0.3$.

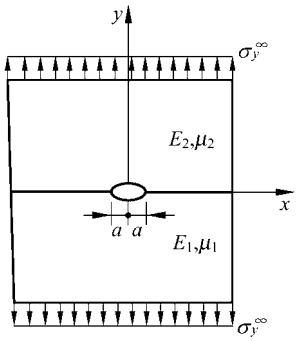

Figure 13.10 An infinite plate in extension with a crack at a bi-material interface

The stress intensity factors of the interface crack are defined as follows:

$$K_{\text{I}} - \text{i}K_{\text{II}} = 2\sqrt{2}\text{e}^{-\pi \text{Im}\,\lambda_1} \lim_{z\to 0} z^{\overline{\lambda}_1} \phi_2'(z)$$

where $\phi_2(z)$ denotes the complex potential function of elasticity, and can be expressed in terms of the stress coefficients $\boldsymbol{\beta}$.

Numerical results are listed in Table 13.8. In comparison with classical solutions[15], all relative errors are within 1%.

In practical computations, the infinite plate is replaced by a $20\text{m} \times 20\text{m}$ plate. The radius of the singular element is taken as $0.08a$, and the first 4 terms of λ are used. It can be seen that the results are basically stable. The accuracy of K_{II} is lower than that of K_{I}. So, for improving the precision of K_{II}, more terms of the eigenvalues are needed.

Table 13.8 Stress intensity factors of a central interface crack in an infinite plate under uniform tension

G_2 / G_1		1	3	10	100	1000
K_{I}	SRM-V2	1.009	0.999	0.981	0.968	0.957
	Reference [15]	1.000	0.988	0.968	0.953	0.952
K_{II}	SRM-V2	0.0	0.0822	0.1289	0.1401	0.1535
	Reference [15]	0.0	0.0724	0.1171	0.1391	0.1415

13.4 Anti-Plane V-Notch Problem in a Bi-Material

This section will discuss the anti-plane V-notch problem (Mode Ⅲ) in a bi-material[16]. Firstly, the stress fields around the notch-tip are derived by the

eigenfunction method; then, the stress intensity factor K_{III} is solved by the sub-region mixed element method. Besides, the anti-plane V-notch problem has already been analyzed by the weight function theory in references [17, 18], and the anti-plane crack problem in a non-homogenous elastic material has also been studied in [19].

13.4.1 The Displacement and Stress Fields around the Notch-Tip

An anti-plane V-notch in a bi-material shown in Fig. 13.11 is considered. Let the interface line of the two materials be the *x*-axis, then equations of two notch sides are $\theta = \theta_1$ and $\theta = \theta_2$, respectively.

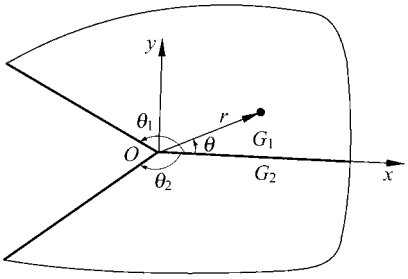

Figure 13.11 An anti-plane V-notch in a bi-material

Under the anti-plane state, only the displacement *w* in the *z*-direction exists, so the stresses can be expressed in terms of displacement as follows:

$$\tau_{rzi} = G_i \frac{\partial w_i}{\partial r}, \quad \tau_{\theta zi} = G_i \frac{1}{r} \frac{\partial w_i}{\partial \theta} \tag{13-47}$$

in which G_i denotes the shear modulus of the material *i*, $i = 1$ and 2.

Ignoring the influences of body forces, the equilibrium equation can be expressed in terms of stresses as follows:

$$\frac{\partial}{\partial r}(r\tau_{rzi}) + \frac{\partial}{\partial \theta}(\tau_{\theta zi}) = 0 \tag{13-48}$$

Substitution of Eq. (13-47) into Eq. (13-48) yields the equilibrium equation expressed in terms of displacement:

$$\frac{\partial^2 w_i}{\partial r^2} + \frac{1}{r}\frac{\partial w_i}{\partial r} + \frac{1}{r^2}\frac{\partial^2 w_i}{\partial \theta^2} = 0 \tag{13-49}$$

w_i can be rewritten as the following form of separated variables

$$w_i = r^{\lambda+1} F_i(\theta, \lambda)$$

Then, from Eq. (13-49), we obtain

$$w_i(r,\theta) = r^{\lambda+1}[A_i \cos(\lambda+1)\theta + B_i \sin(\lambda+1)\theta] \tag{13-50}$$

Assume that there is no external load around the notch-tip, so the boundary conditions of the notch can be expressed as follows:

$$\tau_{z\theta 1}\big|_{\theta=\theta_1} = 0, \quad \tau_{z\theta 2}\big|_{\theta=\theta_2} = 0$$

And, the continuity conditions of displacements and stresses between the two materials are

$$w_1\big|_{\theta=0} = w_2\big|_{\theta=0}, \quad \tau_{z\theta 1}\big|_{\theta=0} = \tau_{z\theta 2}\big|_{\theta=0}$$

By Eqs. (13-47) and (13-50), we can obtain

$$\left.\begin{aligned} &-A_1 \sin(\lambda+1)\theta_1 + B_1 \cos(\lambda+1)\theta_1 = 0 \\ &-A_2 \sin(\lambda+1)\theta_2 + B_2 \cos(\lambda+1)\theta_2 = 0 \\ &A_1 = A_2, \quad G_1 B_1 = G_2 B_2 \end{aligned}\right\} \tag{13-51}$$

In order to obtain nonzero solutions from the original problem, the coefficient determinant of Eq. (13-51) must be zero, then we have

$$G_1 \sin(\lambda+1)\theta_1 \cos(\lambda+1)\theta_2 - G_2 \sin(\lambda+1)\theta_2 \cos(\lambda+1)\theta_1 = 0 \tag{13-52}$$

Equation (13-52) is the eigenequaiton of the anti-plane V-notch in a bi-material. In general, a series of solutions for λ can be solved by the Muller iteration method. For the following special cases:

$$\text{If } G_1 = G_2, \quad \lambda_n + 1 = n\pi/(\theta_1 - \theta_2) \quad (n = 1, 2, \cdots)$$

$$\text{If } \theta_1 = -\theta_2, \quad \lambda_n + 1 = n\pi/(2\theta_1) \quad (n = 1, 2, \cdots)$$

The singularities of stresses and strains will increase with the decrease of the corresponding λ. Hence, the influence of the minimum eigenvalue λ_1 is dominant for the singularity of notch-tip. If only λ_1 is considered, the displacement and stress fields around the notch-tip can be derived from Eq. (13-51):

$$\left.\begin{aligned} w_i &= K_{\mathrm{III}} \frac{(2\pi)^{\lambda_1} r^{\lambda_1+1}}{G_i(\lambda_1+1)} \frac{\cos[(\lambda_1+1)(\theta_i-\theta)]}{\sin[(\lambda_1+1)\theta_i]} \\ \tau_{zri} &= K_{\mathrm{III}} (2\pi r)^{\lambda_1} \frac{\cos[(\lambda_1+1)(\theta_i-\theta)]}{\sin[(\lambda_1+1)\theta_i]} \\ \tau_{\theta zi} &= K_{\mathrm{III}} (2\pi r)^{\lambda_1} \frac{\sin[(\lambda_1+1)(\theta_i-\theta)]}{\sin[(\lambda_1+1)\theta_i]} \end{aligned}\right\} \quad (i = 1, 2) \tag{13-53}$$

in which K_{III} is the stress intensity factor of the anti-plane V-notch in a bi-material, and is defined as:

$$K_{\mathrm{III}} = \lim_{r=0} \frac{1}{(2\pi r)^{\lambda_1}} \tau_{\theta zi}\big|_{\theta=0} \tag{13-54}$$

If let $G_1 = G_2$ and $\theta_1 = -\theta_2 = \pi$ in Eq. (13-53), the displacement and stress fields of the mode Ⅲ crack in homogenous material can then be obtained, and they are in agreement with those given in reference [20].

Equation (13-53) gives the dominant term of the displacement and stress fields around the notch-tip, in which an undetermined parameter K_{III} is included. And, Eq. (13-53) can be rewritten as:

$$w_i = K_{\mathrm{III}} \tilde{w}_i, \quad \tau_{zri} = K_{\mathrm{III}} \tilde{\tau}_{zri}, \quad \tau_{\theta zi} = K_{\mathrm{III}} \tilde{\tau}_{\theta zi} \tag{13-55}$$

13.4.2 The Sub-Region Mixed Element Method

The energy functional of the sub-region mixed variational principle is still given by Eq. (12-5), i.e.,

$$\Pi = \Pi_{\mathrm{p}} - \Pi_{\mathrm{c}} + H_{\mathrm{pc}} \tag{13-56}$$

in which the stress parameter K_{III} of the complementary energy region and the nodal displacements $\boldsymbol{\delta}$ of the potential energy region are the basic unknowns.

(1) The total potential energy Π_{p} of the potential energy region

$$\Pi_{\mathrm{p}} = \frac{1}{2}\boldsymbol{\delta}^{\mathrm{T}}\boldsymbol{K}\boldsymbol{\delta} - \boldsymbol{\delta}^{\mathrm{T}}\boldsymbol{P} = \frac{1}{2}\sum_{k=1}^{n}\sum_{j=1}^{n} K_{kj} w_k w_j - \sum_{j=1}^{n} P_j w_j \tag{13-57}$$

where n is the total number of the nodes of the displacement-based elements in the potential energy region; $\boldsymbol{K}$ is the stiffness matrix; $\boldsymbol{P}$ is the equivalent nodal load vector; $\boldsymbol{\delta}$ is the nodal displacement vector:

$$\boldsymbol{\delta} = [w_1 \quad w_2 \quad \cdots \quad w_n]^{\mathrm{T}}$$

(2) The total complementary energy Π_{c} of the complementary energy region

The complementary energy region A_{c} is composed of two materials, which are denoted as $A_{\mathrm{c}1}$ and $A_{\mathrm{c}2}$, respectively. Thus, the complementary energy Π_{c} of the complementary energy region is

$$\Pi_{\mathrm{c}} = \frac{1}{2G_1}\iint_{A_{\mathrm{c}1}} (\tau_{rz1}^2 + \tau_{\theta z1}^2)\mathrm{d}A + \frac{1}{2G_2}\iint_{A_{\mathrm{c}2}} (\tau_{rz2}^2 + \tau_{\theta z2}^2)\mathrm{d}A$$

Substitution of Eq. (13-53) into the above equation yields

$$\Pi_{\mathrm{c}}=\frac{K_{\mathrm{III}}^2}{2G_1\sin^2(\lambda_1+1)\theta_1}\iint_{A_{\mathrm{c}1}}(2\pi r)^{2\lambda_1}\,\mathrm{d}A+\frac{K_{\mathrm{III}}^2}{2G_2\sin^2(\lambda_1+1)\theta_2}\iint_{A_{\mathrm{c}2}}(2\pi r)^{2\lambda_1}\,\mathrm{d}A$$

If the complementary energy region is assumed as a sectorial region with radius r_{c}, then we have

$$\Pi_{\mathrm{c}}=\frac{1}{2}K_{\mathrm{III}}^2V \tag{13-58}$$

where

$$V=\frac{(2\pi)^{2\lambda_1}r_{\mathrm{c}}^{2\lambda_1+2}}{2(\lambda_1+1)}\left[\frac{\theta_1}{G_1\sin^2(\lambda_1+1)\theta_1}-\frac{\theta_2}{G_2\sin^2(\lambda_1+1)\theta_2}\right] \tag{13-59}$$

(3) The additional energy H_{pc} on the interface

The interface line S_{pc} is composed of two segments S_{pc1} and S_{pc2}. The total number of the nodes on the interface is n_1, and the nodal displacement vector on the interface is

$$\overline{\boldsymbol{\delta}}=[w_1\quad w_2\quad\cdots\quad w_{n_1}]^{\mathrm{T}}$$

Then, the additional energy H_{pc} on the interface is

$$H_{\mathrm{pc}}=\int_{S_{\mathrm{pc1}}}\tau_{rz1}\overline{w}\mathrm{d}s+\int_{S_{\mathrm{pc2}}}\tau_{rz2}\overline{w}\mathrm{d}s \tag{13-60}$$

And, the displacement $\overline{w}$ on the interface can be expressed in terms of the nodal displacement vector $\overline{\boldsymbol{\delta}}$ and shape functions $\overline{\boldsymbol{N}}$ as

$$\overline{w}=\sum_{j=1}^{n_1}\overline{N}_jw_j \tag{13-61}$$

Substituting the above equation into Eq. (13-60), H_{pc} can be expressed in terms of K_{III} and $\overline{\boldsymbol{\delta}}$ as

$$H_{\mathrm{pc}}=K_{\mathrm{III}}\sum_{j=1}^{n_1}h_jw_j \tag{13-62}$$

where

$$h_j=\int_{S_{\mathrm{pc1}}}\tau_{rz1}\overline{N}_j\mathrm{d}s+\int_{S_{\mathrm{pc2}}}\tau_{rz2}\overline{N}_j\mathrm{d}s \tag{13-63}$$

(4) The energy stationary condition

Substituting Eqs. (13-57), (13-58) and (13-62) into Eq. (13-56), the energy Π can be expressed in terms of the basic unknowns K_{III} and $\boldsymbol{\delta}$ as

$$\Pi=\frac{1}{2}\sum_{k=1}^{n}\sum_{j=1}^{n}k_{kj}w_kw_j-\sum_{j=1}^{n}P_jw_j-\frac{1}{2}K_{\mathrm{III}}^2V+K_{\mathrm{III}}\sum_{j=1}^{n_1}h_jw_j \tag{13-64}$$

From the stationary condition $\dfrac{\partial \Pi}{\partial w_j}=0$, we obtain

$$\left.\begin{aligned}&\sum_{k=1}^{n}K_{kj}w_k+K_{\mathrm{III}}h_j=P_j\quad(j=1,2,\cdots,n_1)\\&\sum_{k=1}^{n}K_{kj}w_k=P_j\quad(j=n_1+1,\cdots,n)\end{aligned}\right\}\tag{13-65}$$

From $\dfrac{\partial \Pi}{\partial K_{\mathrm{III}}}=0$, we obtain

$$-K_{\mathrm{III}}V+\sum_{j=1}^{n_1}h_jw_j=0\tag{13-66}$$

By substituting Eq. (13-66) into the first expression in Eq. (13-65), K_{III} can be eliminated, and $\boldsymbol{\delta}=[w_1\quad w_2\quad\cdots\quad w_n]^{\mathrm{T}}$ can first be solved. Then, K_{III} can be solved from Eq. (13-66).

The sub-region mixed element method for the anti-plane V-notch problem in a bi-material is denoted as SRM-V3.

Example 13.5 Evaluate the stress intensity factor K_{III} of an infinite V-notch in a bi-material. Let the interface of the two materials be the sectrix line for the opening angle of the V-notch, and a pair of concentrated forces P with reverse directions act on the notch boundary (Fig. 13.12).

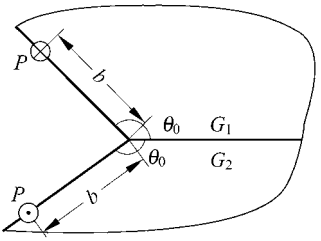

Figure 13.12 An infinite V-notch in a bi-material

The computational formula of K_{III} obtained by weight function method in [17] is

$$K_{\mathrm{III}}=(2\pi)^{1-\frac{\pi}{2\theta_0}}\frac{P}{\theta_0 b^{1-\frac{\pi}{2\theta_0}}}\tag{13-67}$$

where b is the distance from load P to the notch-tip.

The results of the stress intensity factor K_{III} calculated by the sub-region

mixed element method are listed in Table 13.9. And for comparison, the results of [17] are also given. Here, $\theta_0 = \frac{3}{4}\pi$ and $b = 10\text{m}$.

Table 13.9 Results of K_{III} with different radius r_c of the complementary energy region

r_c/b	0.2	0.1	0.075	0.05	0.01	Reference [17]
K_{III} / P	0.740	0.761	0.794	0.812	0.832	0.783
Error (%)	– 5.25	– 2.82	1.39	3.68	6.23	

It can be seen from Table 13.9 that, when $\frac{r_c}{b} = 0.075$, the accuracy of the present method (SRM-V3) is the best. And, when $0.01 \leqslant \frac{r_c}{b} \leqslant 0.2$, the numerical results are relatively stable. By increasing the number of the displacement-based elements outside the interface S_{pc}, the stress continuity on the interface can be improved, then the computational accuracy of K_{III} can also be improved.

13.5 V-Notch Problem in Reissner Plate

This section will discuss the V-notch problem in a thick plate[3]. Since limitations may happen for the crack and V-notch problems in plate bending if the Kirchhoff thin plate theory is used, the Reissner plate theory which considers the influence of shear deformation is adopted here. Firstly, the eigenequations and their solutions for the V-notch problem in the Reissner plate are derived; then, the expressions of stress and displacement fields around the notch-tip in the Reissner plate are derived; finally, the stress intensity factor is solved by the sub-region mixed element method.

13.5.1 The Eigenequations and Eigenvalues of V-Notch Problem in Reissner Plate

1. Fundamental equations

As shown in Fig. 13.13, a bending plate with a notch is considered, and the notch-tip is taken as the origin of the coordinate system. By using the Reissner theory and polar coordinates, the fundamental equations of the thick plate can be expressed in terms of 3 generalized displacements ψ_r, ψ_θ and w as

$$\left.\begin{aligned}
&D\left[\frac{\partial^2\psi_r}{\partial r^2}+\frac{1}{r}\frac{\partial\psi_r}{\partial r}-\frac{\psi_r}{r^2}+\frac{1-\mu}{2}\frac{\partial^2\psi_r}{r^2\partial\theta^2}+\frac{1+\mu}{2}\frac{1}{r}\frac{\partial^2\psi_\theta}{\partial r\partial\theta}-\frac{3-\mu}{2}\frac{\partial\psi_\theta}{r^2\partial\theta}\right]\\
&\qquad+C\left(\frac{\partial w}{\partial r}-\psi_r\right)=0\\
&D\left[\frac{1+\mu}{2}\frac{1}{r}\frac{\partial^2\psi_r}{\partial r\partial\theta}+\frac{3-\mu}{2}\frac{1}{r^2}\frac{\partial\psi_r}{\partial\theta}+\frac{1-\mu}{2}\frac{\partial^2\psi_\theta}{\partial r^2}+\frac{1-\mu}{2}\frac{1}{r}\frac{\partial\psi_\theta}{\partial r}+\frac{1}{r^2}\frac{\partial^2\psi_\theta}{\partial\theta^2}-\frac{1-\mu}{2}\frac{\psi_\theta}{r^2}\right]\\
&\qquad+C\left(\frac{1}{r}\frac{\partial w}{\partial\theta}-\psi_\theta\right)=0\\
&C\left[\frac{\partial^2 w}{\partial r^2}+\frac{1}{r}\frac{\partial w}{\partial r}+\frac{1}{r^2}\frac{\partial^2 w}{\partial\theta^2}-\left(\frac{\partial\psi_r}{\partial r}+\frac{\psi_r}{r}+\frac{1}{r}\frac{\partial\psi_\theta}{\partial\theta}\right)\right]+p=0
\end{aligned}\right\} \tag{13-68}$$

where ψ_r and ψ_θ are rotating angles of straight lines which are perpendicular to the middle plane before deformation. ψ_r is the rotating angle in the *rz*-plane, and is positive if rotates from *r*-axis to *z*-axis; ψ_θ is the rotating angle in the θz-plane, and is positive if rotates from θ-direction to *z*-axis; *w* is the deflection. *D* and *C* are bending and shearing stiffness, respectively,

$$D=\frac{Eh^3}{12(1-\mu^2)},\quad C=\frac{5}{6}Gh$$

in which *E* is the Young's modulus; *G* is the shear modulus; μ is the Poisson's ratio; *h* is the thickness of the plate; *p* is the density of the external load.

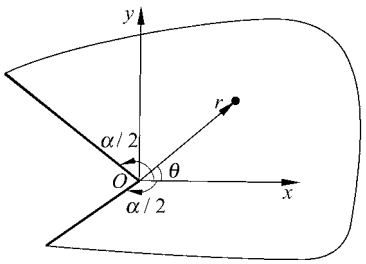

Figure 13.13 V-notch problem in plate bending

The relations between internal forces and displacements are as follows:

$$\left.\begin{aligned} M_r &= -D\left[\frac{\partial \psi_r}{\partial r}+\mu\left(\frac{1}{r}\frac{\partial \psi_\theta}{\partial \theta}+\frac{\psi_r}{r}\right)\right] \\ M_\theta &= -D\left[\frac{1}{r}\frac{\partial \psi_\theta}{\partial \theta}+\frac{\psi_r}{r}+\mu\frac{\partial \psi_r}{\partial r}\right] \\ M_{r\theta} &= -D\frac{1-\mu}{2}\left(\frac{1}{r}\frac{\partial \psi_r}{\partial \theta}+\frac{\partial \psi_\theta}{\partial r}-\frac{\psi_\theta}{r}\right) \\ Q_r &= C\left(\frac{\partial w}{\partial r}-\psi_r\right) \\ Q_\theta &= C\left(\frac{1}{r}\frac{\partial w}{\partial \theta}-\psi_\theta\right) \end{aligned}\right\} \tag{13-69}$$

The boundary conditions of the notch are

$$M_\theta = M_{r\theta} = Q_\theta = 0 \quad (\theta = \pm\alpha/2) \tag{13-70}$$

2. Eigenexpansions and eigenequations

ψ_r , ψ_θ and w can be expanded as follows:

$$\left.\begin{aligned} \psi_r &= \sum_j\sum_n r^{\lambda_j+n}a_{nj}(\theta,\lambda_j) \\ \psi_\theta &= \sum_j\sum_n r^{\lambda_j+n}b_{nj}(\theta,\lambda_j) \\ w &= \sum_j\sum_n r^{\lambda_j+n}c_{nj}(\theta,\lambda_j) \end{aligned}\right\} \tag{13-71}$$

Substitution of Eq. (13-71) into Eq. (13-68) yields

$$\sum_j\sum_n\left\{D\left[((\lambda_j+n)^2-1)a_{nj}+\frac{1-\mu}{2}a''_{nj}+\left(\frac{1+\mu}{2}(\lambda_j+n)-\frac{3-\mu}{2}\right)b'_{nj}\right]r^{\lambda_j+n-2}\right.$$
$$\left.+C(\lambda_j+n)c_{nj}\lambda^{\lambda_j+n-1}-Ca_{nj}r^{\lambda_j+n}\right\}=0$$

$$\sum\sum\left\{D\left[\left(\frac{1+\mu}{2}(\lambda_j+n)+\frac{3-\mu}{2}\right)a'_{nj}+\frac{1-\mu}{2}((\lambda_j+n)^2-1)b_{nj}+b''_{nj}\right]r^{\lambda_j+n-2}\right.$$
$$\left.+Cc'_{nj}r^{\lambda_j+n-1}-Cb_{nj}r^{\lambda_j+n}\right\}=0$$

$$\sum\sum\{[(\lambda_j+n)^2c_{nj}+c''_{nj}]r^{\lambda_j+n-2}-[(\lambda_j+n+1)a_{nj}+b'_{nj}]r^{\lambda_j+n}\}=0$$

in which $a'_{nj}=\dfrac{\partial a_{nj}}{\partial\theta}$, and others can be obtained by analogy. In the above equation

set, if we let the sum of the coefficients of r with the same power order be zero, equation sets with various orders can be obtained. For instance, the lowest order equation set (called zero-order equation set) is formed by letting the sum of the coefficients of r^{λ_j-2} terms be zero, i.e.,

$$\left.\begin{aligned}
&(\lambda_j^2-1)a_{0j}+\frac{1-\mu}{2}a_{0j}''+\left(\frac{1+\mu}{2}\lambda_j-\frac{3-\mu}{2}\right)b_{0j}'=0\\
&\left(\frac{1+\mu}{2}\lambda_j+\frac{3-\mu}{2}\right)a_{0j}'+\frac{1-\mu}{2}(\lambda_j^2-1)b_{0j}+b_{0j}''=0\\
&c_{0j}''+\lambda_j^2 c_{0j}=0
\end{aligned}\right\} \tag{13-72}$$

This is a homogenous ordinary differential equation set about a_{0j}, b_{0j} and c_{0j}. And, if we let the sum of the coefficients of r^{λ_j-1} terms be zero, the first-order equation set, which is a homogenous ordinary differential equation set about (a_{1j}, b_{1j}, c_{1j}) and (a_{0j}, b_{0j}, c_{0j}), can be established. Then from this set, a_{1j}, b_{1j} and c_{1j} can be solved. According to this step, equation set of any order can be obtained, and the corresponding coefficients a_{nj}, b_{nj} and c_{nj} can be solved.

The solution strategy for the zero-order equation set (13-72) is discussed in detail as follows. Its solutions can be expressed by

$$\left.\begin{aligned}
a_{0j}&=A_{0j}\cos(\lambda_j+1)\theta+B_{0j}\sin(\lambda_j+1)\theta+C_{0j}\cos(\lambda_j-1)\theta+D_{0j}\sin(\lambda_j-1)\theta\\
b_{0j}&=B_{0j}\cos(\lambda_j+1)\theta-A_{0j}\sin(\lambda_j+1)\theta+K_{0j}D_{0j}\cos(\lambda_j-1)\theta-K_{0j}C_{0j}\sin(\lambda_j-1)\theta\\
c_{0j}&=E_{0j}\cos\lambda_j\theta+F_{0j}\sin\lambda_j\theta
\end{aligned}\right\} \tag{13-73}$$

in which the parameter K_{0j} is

$$K_{0j}=\frac{(1+\mu)\lambda_j+(3-\mu)}{(1+\mu)\lambda_j-(3-\mu)}$$

A_{0j}, B_{0j}, C_{0j}, D_{0j}, E_{0j} and F_{0j} are 6 undetermined coefficients; λ_j is the eigenvalue, and determined by the eigenequation.

The zero-order boundary conditions which a_{0j}, b_{0j} and c_{0j} should satisfy can be derived from the boundary condition Eq. (13-70). Therefore, substitution of Eq. (13-71) into Eq. (13-69) yields the series expressions of the internal forces. Substituting them into Eq. (13-70), the series expressions of the boundary conditions can also be obtained, in which the zero-order boundary conditions are

$$\left.\begin{array}{l} b'_{0j}+(\lambda_j\mu+1)a_{0j}=0 \\ a'_{0j}+(\lambda_j-1)b_{0j}=0 \\ c'_{0j}=0 \end{array}\right\} \quad \left(\theta=\pm\frac{\alpha}{2}\right) \tag{13-74}$$

Substituting Eq. (13-73) into the above equation, the following 6 conditions can be obtained:

$$2\lambda_j(\mu-1)A_{0j}\cos(\lambda_j+1)\frac{\alpha}{2}+2[-K_{0j}(\lambda_j-1)+(1+\lambda_j\mu)]C_{0j}\cos(\lambda_j-1)\frac{\alpha}{2}=0 \tag{13-75a}$$

$$2\lambda_j A_{0j}\sin(\lambda_j+1)\frac{\alpha}{2}+(\lambda_j-1)(K_{0j}+1)C_{0j}\sin(\lambda_j-1)\frac{\alpha}{2}=0 \tag{13-75b}$$

$$2\lambda_j(\mu-1)B_{0j}\sin(\lambda_j+1)\frac{\alpha}{2}+2[-K_{0j}(\lambda_j-1)+(1+\lambda_j\mu)]D_{0j}\sin(\lambda_j-1)\frac{\alpha}{2}=0 \tag{13-75c}$$

$$2\lambda_j B_{0j}\cos(\lambda_j+1)\frac{\alpha}{2}+(\lambda_j-1)(K_{0j}+1)D_{0j}\cos(\lambda_j-1)\frac{\alpha}{2}=0 \tag{13-75d}$$

$$F_{0j}\cos\lambda_j\frac{\alpha}{2}=0 \tag{13-75e}$$

$$E_{0j}\sin\lambda_j\frac{\alpha}{2}=0 \tag{13-75f}$$

This is a homogenous algebraic equation set about 6 undetermined coefficients A_{0j}, B_{0j}, C_{0j}, D_{0j}, E_{0j} and F_{0j}. If the homogenous equation set has nontrivial solutions, its coefficient determinant should be zero, i.e.,

$$(\sin\lambda_j\alpha+\lambda_j\sin\alpha)(\sin\lambda_j\alpha-\lambda_j\sin\alpha)\cos\lambda_j\frac{\alpha}{2}\sin\lambda_j\frac{\alpha}{2}=0 \tag{13-76}$$

This is the eigenequation for the V-notch problem in the Reissner plate, from which a series of eigenvalues λ_j can be determined.

By the way, the eigenequation (13-76) can be decomposed into the following 4 equations:

$$\sin\lambda_j\alpha+\lambda_j\sin\alpha=0 \tag{13-77a}$$

$$\sin\lambda_j\alpha-\lambda_j\sin\alpha=0 \tag{13-77b}$$

$$\cos\lambda_j\frac{\alpha}{2}=0 \tag{13-77c}$$

$$\sin\lambda_j\frac{\alpha}{2}=0 \tag{13-77d}$$

They are corresponding to the following 4 conditions, respectively:

A_{0j} and C_{0j} in Eqs. (13-75a,b) have nontrivial solutions;

B_{0j} and D_{0j} in Eqs. (13-75c,d) have nontrivial solutions;

F_{0j} in Eq. (13-75e) has nontrivial solution;

E_{0j} in Eq. (13-75f) has nontrivial solution.

3. The solution of eigenequation

By comparing the eigenequation (13-76) for the V-notch problem in the Reissner plate with the eigenequations (13-7) and (13-8) for the plane V-notch problem, it can be seen that, besides the first two factors contained in the left side of Eq. (13-76) that are the same as those in Eqs. (13-7) and (13-8), there are still other two factors, $\cos\lambda_j\frac{\alpha}{2}$ and $\sin\lambda_j\frac{\alpha}{2}$, existing here. Hence, the singularities of the V-notches in the Reissner plate and plane problem have some relations, but are different.

By Muller iteration method, all the real and complex roots of Eq. (13-76) can be solved. A series of eigenvalues with various opening angles of notch are listed in Table 13.10.

Along with the decrease of the inner angle of the notch, the minimum eigenvalue λ_1 increases gradually, which means that the singularity at the tip of the notch decreases gradually. When the inner angle of the notch tends to be 180°, the singularity at the tip of the notch will disappear.

For convenience, let us divide the roots of the eigenequation (13-76) into two parts: one is composed of $\{\lambda_1, \lambda_4, \lambda_5, \lambda_8, \cdots\}$, which represents the symmetric part; the other is composed of $\{\lambda_2, \lambda_3, \lambda_6, \lambda_7, \cdots\}$, which represents the antisymmetric part. The coefficients of displacement corresponding to the symmetric part and antisymmetric part are derived in the following, respectively. Furthermore, the expressions of stresses at the tip of the notch can be obtained.

13.5.2 The Internal Force Fields at Notch-Tip in Reissner Plate —the Symmetric Part

The symmetric part is corresponding to the following eigenvalue series:

$$[\lambda_1, \lambda_4, \lambda_5, \lambda_8, \lambda_9, \lambda_{12}, \cdots]$$

which can be divided into two groups, a and b:

$$\text{group a: } [\lambda_1, \lambda_5, \lambda_9, \cdots]$$

$$\text{group b: } [\lambda_4, \lambda_8, \lambda_{12}, \cdots]$$

Table 13.10 The eigenvalues of V-notch in Reissner plate

λ_i \ α	360°		350°		330°		300°		270°		240°	
λ_1	0.500 000	0.0	0.500 053	0.0	0.501 453	0.0	0.512 222	0.0	0.544 484	0.0	0.615 731	0.0
λ_2	0.500 000	0.0	0.514 286	0.0	0.545 455	0.0	0.600 000	0.0	0.666 666	0.0	0.750 000	0.0
λ_3	0.500 000	0.0	0.529 355	0.0	0.598 192	0.0	0.730 901	0.0	0.908 529	0.0	1.148 913	0.0
λ_4	1.000 000	0.0	1.028 571	0.0	1.090 909	0.0	1.200 000	0.0	1.333 333	0.0	1.500 000	0.0
λ_5	1.000 000	0.0	1.058 843	0.0	1.202 157	0.0	1.471 028	0.141 853	1.629 257	0.231 251	1.833 550	0.252 260
λ_6	1.500 000	0.0	1.542 857	0.0	1.636 364	0.0	1.800 000	0.0	2.000 000	0.0	2.250 000	0.0
λ_7	1.500 000	0.0	1.588 609	0.0	1.838 934	0.0	2.074 826	0.229 426	2.301 328	0.315 837	2.589 479	0.348 375
λ_8	2.000 000	0.0	2.057 143	0.0	2.181 818	0.0	2.400 000	0.0	2.666 667	0.0	3.000 000	0.0
λ_9	1.500 000	0.0	1.499 728	0.0	1.490 378	0.0	2.567 762	0.284 901	2.971 844	0.373 931	3.343 717	0.414 037
λ_{10}	2.500 000	0.0	2.571 429	0.0	2.727 273	0.0	3.000 000	0.0	3.333 333	0.0	3.750 000	0.0
λ_{11}	2.000 000	0.0	1.999 107	0.0	1.948 556	0.0	3.279 767	0.326 690	3.641 420	0.418 787	4.096 928	0.464 641
λ_{12}	3.000 000	0.0	3.085 714	0.0	3.272 727	0.0	3.600 000	0.0	4.000 000	0.0	4.500 000	0.0
λ_{13}	2.000 000	0.0	2.118 822	0.0	2.440 492	0.114 207						
λ_{14}	3.500 000	0.0	3.600 000	0.0	3.818 132	0.0						
λ_{15}	2.500 000	0.0	2.649 696	0.0	2.987 005	0.166 741						
λ_{16}	4.000 000	0.0	4.114 286	0.0	4.363 636	0.0						
λ_{17}	2.500 000	0.0	2.497 980	0.0								
λ_{18}	4.500 000	0.0	4.628 571	0.0								
λ_{19}	3.000 000	0.0	2.996 141	0.0								
λ_{20}	5.000 000	0.0	5.142 857	0.0								

The results for the first two orders ($n=0$ and $n=1$) are given as follows.

(1a) $n=0, j=1,5,9,\cdots$

In this case, λ_j satisfies Eq. (13-77a). From Eqs. (13-75a) and (13-75b), we have

$$C_{0j} = m_{0j}\beta_j$$

where

$$m_{0j} = -\frac{2\lambda_j \sin(\lambda_j+1)\dfrac{\alpha}{2}}{(\lambda_j-1)(1+K_{0j})\sin(\lambda_j-1)\dfrac{\alpha}{2}}$$

and β_j represents A_{0j}.

And, from Eqs. (13-75c), (13-75d), (13-75e) and (13-75f), we can obtain

$$B_{0j} = D_{0j} = E_{0j} = F_{0j} = 0$$

Therefore, Eq. (13-73) yields

$$\left.\begin{aligned} a_{0j} &= [\cos(\lambda_j+1)\theta + m_{0j}\cos(\lambda_j-1)\theta]\beta_j \\ b_{0j} &= -[\sin(\lambda_j+1)\theta + K_{0j}m_{0j}\sin(\lambda_j-1)\theta]\beta_j \\ c_{0j} &= 0 \end{aligned}\right\} \tag{13-78}$$

And, the corresponding internal force fields can be written as

$$\left.\begin{aligned} M_r &= -Dr^{\lambda_j-1}\{(1-\mu)\lambda_j\cos(\lambda_j+1)\theta + m_{0j}[(\lambda_j+\mu)-K_{0j}\mu(\lambda_j-1)]\cos(\lambda_j-1)\theta\}\beta_j \\ M_\theta &= -Dr^{\lambda_j-1}\{(\mu-1)\lambda_j\cos(\lambda_j+1)\theta + m_{0j}[1+\lambda_j\mu-K_{0j}(\lambda_j-1)]\cos(\lambda_j-1)\theta\}\beta_j \\ M_{r\theta} &= \frac{D(1-\mu)}{2}r^{\lambda_j-1}[2\lambda_j\sin(\lambda_j+1)\theta + (\lambda_j-1)(1+K_{0j})m_{0j}\sin(\lambda_j-1)\theta]\beta_j \\ Q_r &= -Cr^{\lambda_j}[\cos(\lambda_j+1)\theta + m_{0j}\cos(\lambda_j-1)\theta]\beta_j \\ Q_\theta &= Cr^{\lambda_j}[\sin(\lambda_j+1)\theta + K_{0j}m_{0j}\sin(\lambda_j-1)\theta]\beta_j \end{aligned}\right\} \tag{13-79}$$

(1b) $n=0, j=4,8,12,\cdots$

In this case, λ_j only satisfies Eq. (13-77d). Then, from Eq. (13-75), we have

$$E_{0j} \neq 0, \quad \text{and} \quad A_{0j} = B_{0j} = C_{0j} = D_{0j} = F_{0j} = 0$$

From Eq. (13-73), we obtain

$$a_{0j} = 0, \quad b_{0j} = 0, \quad c_{0j} = \beta_j \cos\lambda_j\theta \tag{13-80}$$

in which β_j represents E_{0j}. And, the corresponding internal force fields are

$$\left.\begin{aligned} &M_r = 0, \quad M_\theta = 0, \quad M_{r\theta} = 0 \\ &Q_r = Cr^{\lambda_j - 1}(\lambda_j \cos\lambda_j\theta)\beta_j, \quad Q_\theta = Cr^{\lambda_j - 1}(-\lambda_j \sin\lambda_j\theta)\beta_j \end{aligned}\right\} \tag{13-81}$$

(2a) $n = 1, j = 1,5,9,\cdots$

When $n = 1$, from Eq. (13.71), we have

$$\psi_r = r^{\lambda_j + 1}a_{1j}, \quad \psi_\theta = r^{\lambda_j + 1}b_{1j}, \quad w = r^{\lambda_j + 1}c_{1j} \tag{13-82}$$

Substituting Eq. (13-82) into Eq. (13-68), and making use of Eq. (13-78), the following solutions can be obtained:

$$\left.\begin{aligned} a_{1j} &= A_{1j}\cos(\lambda_j + 2)\theta + B_{1j}\sin(\lambda_j + 2)\theta + C_{1j}\cos\lambda_j\theta + D_{1j}\sin\lambda_j\theta \\ b_{1j} &= B_{1j}\cos(\lambda_j + 2)\theta - A_{1j}\sin(\lambda_j + 2)\theta + K_{1j}D_{1j}\cos\lambda_j\theta - K_{1j}C_{1j}\sin\lambda_j\theta \\ c_{1j} &= E_{1j}\cos(\lambda_j + 1)\theta + F_{1j}\sin(\lambda_j + 1)\theta + \frac{\lambda_j + 1 - K_{0j}(\lambda_j - 1)}{4\lambda_j}\beta_j\cos(\lambda_j - 1)\theta \end{aligned}\right\} \tag{13-83}$$

where

$$K_{1j} = \frac{(1+\mu)(1+\lambda_j) + (3-\mu)}{(1+\mu)(1+\lambda_j) - (3-\mu)}$$

Substituting Eq. (13-82) into Eq. (13-70) and making use of Eq. (13-78), the corresponding boundary conditions can be derived as follows:

$$\left.\begin{aligned} &b'_{1j} + a_{1j} + \mu(\lambda_j + 1)a_{1j} = 0 \\ &a'_{1j} + \lambda_j b_{1j} = 0 \\ &c'_{1j} + [\sin(\lambda_j + 1)\theta + K_{0j}m_{0j}\sin(\lambda_j - 1)\theta]\beta_j = 0 \end{aligned}\right\} \quad \left(\theta = \pm\frac{\alpha}{2}\right) \tag{13-84}$$

Substitution of Eq. (13-83) into Eq. (13-84) yields:

$$A_{1j} = B_{1j} = C_{1j} = D_{1j} = F_{1j} = 0, \quad E_{1j} = f_{1j}\beta_{1j}$$

where

$$f_{1j} = -\frac{\lambda_j + 1 - K_{0j}(\lambda_j - 1)}{4\lambda_j(\lambda_j + 1)}(\lambda_j - 1)\frac{\sin(\lambda_j - 1)\dfrac{\alpha}{2}}{\sin(\lambda_j + 1)\dfrac{\alpha}{2}}$$

$$+\frac{1}{\lambda_j + 1}\frac{\sin(\lambda_j + 1)\dfrac{\alpha}{2} + K_{0j}m_{0j}\sin(\lambda_j - 1)\dfrac{\alpha}{2}}{\sin(\lambda_j + 1)\dfrac{\alpha}{2}}$$

From Eq. (13-83), we can obtain

$$a_{1j}=0,\quad b_{1j}=0,\quad c_{1j}=[f_{1j}\cos(\lambda_j+1)\theta+g_{1j}\cos(\lambda_j-1)\theta]\beta_j \tag{13-85}$$

where

$$g_{1j}=[\lambda_j+1+K_{0j}(\lambda_j-1)]/4\lambda_j$$

And, the corresponding internal force fields are

$$\left.\begin{aligned}&M_r=0,\quad M_\theta=0,\quad M_{r\theta}=0\\&Q_r=Cr^{\lambda_j}(\lambda_j+1)[f_{1j}\cos(\lambda_j+1)\theta+g_{1j}\cos(\lambda_j-1)\theta]\beta_j\\&Q_\theta=Cr^{\lambda_j}[-(\lambda_j+1)f_{1j}\sin(\lambda_j+1)\theta-(\lambda_j-1)g_{1j}\sin(\lambda_j-1)\theta]\beta_j\end{aligned}\right\} \tag{13-86}$$

(2b) $n=1, j=4,8,12,\cdots$

Substituting Eq. (13-82) into Eq. (13-68) and making use of Eq. (13-80), we can obtain:

$$\left.\begin{aligned}a_{1j}&=A_{1j}\cos(\lambda_j+2)\theta+B_{1j}\sin(\lambda_j+2)\theta+C_{1j}\cos\lambda_j\theta+D_{1j}\sin\lambda_j\theta\\&\quad-\frac{C}{D[\lambda_j(1+\mu)/2+2]}\beta_j\cos\lambda_j\theta\\b_{1j}&=B_{1j}\cos(\lambda_j+2)\theta-A_{1j}\sin(\lambda_j+2)\theta+K_{1j}D_{1j}\cos\lambda_j\theta-K_{1j}C_{1j}\sin\lambda_j\theta\\c_{1j}&=E_{1j}\cos(\lambda_j+1)\theta+F_{1j}\sin(\lambda_j+1)\theta\end{aligned}\right\} \tag{13-87}$$

Substituting Eq. (13-82) into Eq. (13-70) and making use of Eq. (13-80), the corresponding boundary conditions can be obtained:

$$\left.\begin{aligned}&b'_{1j}+a_{1j}+\mu(\lambda_j+1)a_{1j}=0\\&a'_{1j}+\lambda_j b_{1j}=0,\quad c'_{1j}=0\end{aligned}\right\}\quad\left(\theta=\pm\frac{\alpha}{2}\right) \tag{13-88}$$

Substitution of Eq. (13-87) into Eq. (13-88) yields:

$$B_{1j}=D_{1j}=F_{1j}=E_{1j}=0$$

$$A_{1j}=\frac{c_1a_{22}-c_2a_{12}}{a_{11}a_{22}-a_{12}a_{21}}\beta_j=l_{1j}\beta_j,\quad C_{1j}=\frac{c_2a_{11}-c_1a_{21}}{a_{11}a_{22}-a_{12}a_{21}}\beta_j=v_{1j}\beta_j$$

where

$$a_{11}=2(\lambda_j+1)(\mu-1)\cos(\lambda_j+1)\frac{\alpha}{2},\quad a_{12}=2[-K_{1j}\lambda_j+1+\mu(\lambda_j+1)]\cos\lambda_j\frac{\alpha}{2}$$

$$a_{21}=2(\lambda_j+1)\sin(\lambda_j+2)\frac{\alpha}{2},\quad a_{22}=\lambda_j(1+K_{1j})\sin\lambda_j\frac{\alpha}{2}$$

$$c_1=\frac{2C[1+\mu(\lambda_j+1)]}{D[(1+\mu)\lambda_j/2+2]}\cos\lambda_j\frac{\alpha}{2},\quad c_2=\frac{C}{D[(1+\mu)\lambda_j/2+2]}\lambda_j\sin\lambda_j\frac{\alpha}{2}$$

Finally, from Eq. (13-87), we obtain

$$\left.\begin{aligned}a_{1j}&=[\alpha_{1j}\cos\lambda_j\theta+l_{1j}\cos(\lambda_j+2)\theta]\beta_j\\b_{1j}&=-[K_{1j}v_{1j}\sin\lambda_j\theta+l_{1j}\sin(\lambda_j+2)\theta]\beta_j\\c_{1j}&=0\end{aligned}\right\}\tag{13-89}$$

where

$$\alpha_{1j}=v_{1j}-\frac{C}{D[\lambda_j(1+\mu)/2+2]}$$

And, the corresponding internal force fields are

$$\left.\begin{aligned}M_r&=-Dr^{\lambda_j}\{[\alpha_{1j}(\lambda_j+1+\mu)-K_{1j}v_{1j}\mu\lambda_j]\cos\lambda_j\theta\\&\quad+[l_{1j}(\lambda_j+1+\mu)-\mu l_{1j}(\lambda_j+2)]\cos(\lambda_j+2)\theta\}\beta_j\\M_\theta&=-Dr^{\lambda_j}\{[\alpha_{1j}(\lambda_j\mu+\mu+1)-K_{1j}v_{1j}\lambda_j]\cos\lambda_j\theta\\&\quad+[l_{1j}(\lambda_j\mu+\mu+1)-l_{1j}(\lambda_j+2)]\cos(\lambda_j+2)\theta\}\beta_j\\M_{r\theta}&=\frac{D(1-\mu)}{2}r^{\lambda_j}[\lambda_j(\alpha_{1j}+K_{1j}v_{1j})\sin\lambda_j\theta+2(\lambda_j+1)l_{1j}\sin(\lambda_j+2)\theta]\beta_j\\Q_r&=-Cr^{\lambda_j+1}[\alpha_{1j}\cos\lambda_j\theta+l_{1j}\cos(\lambda_j+2)\theta]\beta_j\\Q_\theta&=Cr^{\lambda_j+1}[K_{1j}v_{1j}\sin\lambda_j\theta+l_{1j}\sin(\lambda_j+2)\theta]\beta_j\end{aligned}\right\}\tag{13-90}$$

13.5.3 The Internal Force Fields at Notch-Tip in Reissner Plate —the Antisymmetric Part

The antisymmetric part is corresponding to the following eigenvalue series:

$$[\lambda_2,\lambda_3,\lambda_6,\lambda_7,\lambda_{10},\lambda_{11},\cdots]$$

which can also be divided into two groups, a and b:

$$\text{group a: } [\lambda_2, \lambda_6, \lambda_{10}, \cdots]$$

$$\text{group b: } [\lambda_3, \lambda_7, \lambda_{11}, \cdots]$$

The results for the first two orders ($n = 0$ and $n = 1$) are given as follows.

(1a) $n = 0, \quad j = 2,6,10, \cdots$

$$a_{0j} = 0, \quad b_{0j} = 0, \quad c_{0j} = \beta_j \sin \lambda_j \theta \tag{13-91}$$

The corresponding internal force fields are

$$\left.\begin{aligned} &M_r = 0, \quad M_\theta = 0, \quad M_{r\theta} = 0 \\ &Q_r = C\lambda_j r^{\lambda_j - 1} \beta_j \sin \lambda_j \theta, \quad Q_\theta = C\lambda_j r^{\lambda_j - 1} \beta_j \cos \lambda_j \theta \end{aligned}\right\} \tag{13-92}$$

(1b) $n = 0, j = 3,7,11, \cdots$

$$\left.\begin{aligned} a_{0j} &= [\sin(\lambda_j + 1)\theta + m'_{0j} \sin(\lambda_j - 1)\theta]\beta_j \\ b_{0j} &= [\cos(\lambda_j + 1)\theta + K_{0j} m'_{0j} \cos(\lambda_j - 1)\theta]\beta_j \\ c_{0j} &= 0 \end{aligned}\right\} \tag{13-93}$$

where

$$m'_{0j} = -\frac{2\lambda_j \cos(\lambda_j + 1)\dfrac{\alpha}{2}}{(\lambda_j - 1)(1 + K_{0j})\cos(\lambda_j - 1)\dfrac{\alpha}{2}}$$

The corresponding internal force fields are

$$\left.\begin{aligned} M_r &= -Dr^{\lambda_j - 1}\{(1-\mu)\lambda_j \sin(\lambda_j + 1)\theta + m'_{0j}[(\lambda_j + \mu) - K_{0j}\mu(\lambda_j - 1)]\sin(\lambda_j - 1)\theta\}\beta_j \\ M_\theta &= -Dr^{\lambda_j - 1}\{(\mu-1)\lambda_j \sin(\lambda_j + 1)\theta + m'_{0j}[1 + \lambda_j\mu - K_{0j}(\lambda_j - 1)]\sin(\lambda_j - 1)\theta\}\beta_j \\ M_{r\theta} &= -\frac{D(1-\mu)}{2} r^{\lambda_j - 1}\{2\lambda_j \cos(\lambda_j + 1)\theta + m'_{0j}(\lambda_j - 1)(1 + K_{0j})\cos(\lambda_j - 1)\theta\}\beta_j \\ Q_r &= -Cr^{\lambda_j}[\sin(\lambda_j + 1)\theta + m'_{0j}\sin(\lambda_j - 1)\theta]\beta_j \\ Q_\theta &= -Cr^{\lambda_j}[\cos(\lambda_j + 1)\theta + m'_{0j}K_{0j}\cos(\lambda_j - 1)\theta]\beta_j \end{aligned}\right\} \tag{13-94}$$

(2a) $n = 1, j = 2,6,10, \cdots$

$$\left.\begin{aligned} a_{1j} &= [a'_{1j}\sin\lambda_j\theta + l'_{1j}\sin(\lambda_j+2)\theta]\beta_j \\ b_{1j} &= [l'_{1j}\cos(\lambda_j+2)\theta + K_{1j}v'_{1j}\cos\lambda_j\theta]\beta_j \\ c_{1j} &= 0 \end{aligned}\right\} \tag{13-95}$$

where

$$l'_{1j} = \frac{c'_1a'_{22} - c'_2a'_{12}}{a'_{11}a'_{22} - a'_{12}a'_{21}},\quad v'_{1j} = \frac{c'_2a'_{11} - c'_1a'_{21}}{a'_{11}a'_{22} - a'_{12}a'_{21}}$$

$$a'_{11} = 2(\lambda_j+1)(\mu-1)\sin(\lambda_j+2)\frac{\alpha}{2}$$

$$a'_{12} = 2[-K_{1j}\lambda_j + 1 + \mu(\lambda_j+1)]\sin\lambda_j\frac{\alpha}{2}$$

$$a'_{21} = 2(\lambda_j+1)\cos(\lambda_j+2)\frac{\alpha}{2},\quad a'_{22} = \lambda_j(1+K_{1j})\cos\lambda_j\frac{\alpha}{2}$$

$$c'_1 = \frac{2[1+\mu(\lambda_j+1)]C}{D\left(\dfrac{1+\mu}{2}\lambda_j+2\right)}\sin\lambda_j\frac{\alpha}{2},\quad c'_2 = \frac{C}{D\left(\dfrac{1+\mu}{2}\lambda_j+2\right)}\lambda_j\cos\lambda_j\frac{\alpha}{2}$$

$$\alpha'_{1j} = v'_{1j} - \frac{C}{D[\lambda_j(1+\mu)/2+2]}$$

The corresponding internal force fields are

$$\left.\begin{aligned} M_r &= -Dr^{\lambda_j}\{[\alpha'_{1j}(\lambda_j+1+\mu) - K_{1j}v'_{1j}\mu\lambda_j]\sin\lambda_j\theta \\ &\quad + [l'_{1j}(\lambda_j+1+\mu) - \mu l'_{1j}(\lambda_j+2)]\sin(\lambda_j+2)\theta\}\beta_j \\ M_\theta &= -Dr^{\lambda_j}\{[\alpha'_{1j}(\lambda_j\mu+\mu+1) - K_{1j}v'_{1j}\lambda_j]\sin\lambda_j\theta \\ &\quad + [l'_{1j}(\lambda_j\mu+\mu+1) - l'_{1j}(\lambda_j+2)]\sin(\lambda_j+2)\theta\}\beta_j \\ M_{r\theta} &= -\frac{D(1-\mu)}{2}r^{\lambda_j}\{[\alpha'_{1j}\lambda_j + \lambda_jK_{1j}v'_{1j}]\cos\lambda_j\theta + 2l'_{1j}(\lambda_j+1)\cos(\lambda_j+2)\theta\}\beta_j \\ Q_r &= -Cr^{\lambda_j+1}[\alpha'_{1j}\sin\lambda_j\theta + l'_{1j}\sin(\lambda_j+2)\theta]\beta_j \\ Q_\theta &= -Cr^{\lambda_j+1}[l'_{1j}\cos(\lambda_j+2)\theta + K_{1j}v'_{1j}\cos\lambda_j\theta]\beta_j \end{aligned}\right\} \tag{13-96}$$

(2b) $n=1, j=3,7,11,\cdots$

$$a_{1j}=0,\quad b_{1j}=0,\quad c_{1j}=[f'_{1j}\sin(\lambda_j+1)\theta + g'_{1j}\sin(\lambda_j-1)\theta]\beta_j \tag{13-97}$$

where

$$f'_{1j} = -\frac{\lambda_j + 1 - K_{0j}(\lambda_j - 1)}{4\lambda_j(\lambda_j + 1)}(\lambda_j - 1)m'_{0j}\frac{\cos(\lambda_j - 1)\dfrac{\alpha}{2}}{\cos(\lambda_j + 1)\dfrac{\alpha}{2}}$$

$$+\frac{\cos(\lambda_j + 1)\alpha + K_{0j}m'_{0j}\cos(\lambda_j - 1)\dfrac{\alpha}{2}}{(\lambda_j + 1)\cos(\lambda_j + 1)\dfrac{\alpha}{2}}$$

$$g'_{1j} = m'_{1j}[\lambda_j + 1 - K_{0j}(\lambda_j - 1)]/4\lambda_j$$

The corresponding internal force fields are

$$\left.\begin{aligned} &M_r = 0, \quad M_\theta = 0, \quad M_{r\theta} = 0 \\ &Q_r = C(\lambda_j + 1)r^{\lambda_j}[f'_{1j}\sin(\lambda_j + 1)\theta + g'_{1j}\sin(\lambda_j - 1)\theta]\beta_j \\ &Q_\theta = Cr^{\lambda_j}[(\lambda_j + 1)f'_{1j}\cos(\lambda_j + 1)\theta + (\lambda_j - 1)g'_{1j}\cos(\lambda_j - 1)\theta]\beta_j \end{aligned}\right\} \quad (13\text{-}98)$$

The expressions for the zero and first order internal force fields have been given above. According to the above process, some higher order solutions can be derived.

When $\alpha = 2\pi$, the V-notch problem will degenerate into the crack problem. The solution of the internal force fields around the crack-tip in the Reissner plate given in reference [21] can be treated as a special case of the solution in this section.

From the above derived expressions of the internal force fields around the notch-tip, it is found that, around the notch-tip, the order of singularity of the transverse shear stresses τ_{rz} and $\tau_{\theta z}$ is different from that of stresses σ_r, σ_θ and $\tau_{r\theta}$, the former is $r^{\lambda_2 - 1}$ while the latter is $r^{\lambda_1 - 1}$. Only when the opening angle $\alpha = 2\pi$ (crack problem), since $\lambda_1 = \lambda_2 = 0.5$, the order of singularity of τ_{rz} and $\tau_{\theta z}$ will be the same as that of σ_r, σ_θ and $\tau_{r\theta}$, which is identical to that in reference [22].

13.5.4 The Sub-Region Mixed Element Method

Now, the sub-region mixed element method is used to analyze the plane V-notch problem in thick plate. The sectorial region centered at the notch-tip is taken as the complementary energy region (C-region), and the outside of the C-region is the potential energy region (P-region). The P-region is divided by the 8-node isoparametric thick plate elements, and its nodal displacements $\boldsymbol{\delta}$ are the undetermined displacement parameters. The above solutions of the internal force fields around the notch-tip can be taken as the internal force fields of the C-region, which can be written as

$$\left.\begin{aligned} \boldsymbol{M} &= \boldsymbol{S}_{\mathrm{b}}\boldsymbol{\beta} \\ \boldsymbol{Q} &= \boldsymbol{S}_{\mathrm{s}}\boldsymbol{\beta} \end{aligned}\right\} \quad (13\text{-}99)$$

where $\boldsymbol{M}=[M_x \quad M_y \quad M_{xy}]^{\mathrm{T}}$ are the bending and twisting moments; $\boldsymbol{Q}=[Q_x \quad Q_y]^{\mathrm{T}}$ are the transverse shear forces; $\boldsymbol{\beta}$ are the undetermined internal force parameters; $\boldsymbol{S}_{\mathrm{b}}$ and $\boldsymbol{S}_{\mathrm{s}}$ are formed by the combination of the internal forces around the notch-tip.

The undetermined parameters $\boldsymbol{\delta}$ and $\boldsymbol{\beta}$ can be determined by the stationary condition of the sub-region mixed variational principle.

The energy functional of the sub-region mixed variational principle is still given by Eq. (12-5), i.e.,

$$\Pi=\Pi_{\mathrm{p}}-\Pi_{\mathrm{c}}+H_{\mathrm{pc}} \tag{13-100}$$

(1) The total potential energy Π_{p} of the P-region (see Eq. (12-6))

$$\Pi_{\mathrm{p}}=\frac{1}{2}\boldsymbol{\delta}^{\mathrm{T}}\boldsymbol{K}\boldsymbol{\delta}-\boldsymbol{\delta}^{\mathrm{T}}\boldsymbol{P} \tag{13-101}$$

in which $\boldsymbol{K}$ and $\boldsymbol{P}$ are the stiffness matrix and the equivalent nodal load vector, respectively.

(2) The total complementary energy Π_{c} of the C-region

The total complementary energy Π_{c} of the C-region in the thick plate is composed of two parts, bending strain complementary energy and shearing strain complementary energy (see Eq. (12-55)):

$$\Pi_{\mathrm{c}}=\frac{1}{2}\iint_{A_{\mathrm{c}}}(\boldsymbol{M}^{\mathrm{T}}\boldsymbol{D}_{\mathrm{b}}^{-1}\boldsymbol{M}+\boldsymbol{Q}^{\mathrm{T}}\boldsymbol{D}_{\mathrm{s}}^{-1}\boldsymbol{Q})\mathrm{d}A \tag{13-102}$$

Substitution of Eq. (13-99) into the above equation yields

$$\Pi_{\mathrm{c}}=\frac{1}{2}\boldsymbol{\beta}^{\mathrm{T}}\boldsymbol{F}\boldsymbol{\beta} \tag{13-103}$$

where $\boldsymbol{F}$ is the flexibility matrix (see Eq. (12-57)):

$$\boldsymbol{F}=\iint_{A_{\mathrm{c}}}(\boldsymbol{S}_{\mathrm{b}}^{\mathrm{T}}\boldsymbol{D}_{\mathrm{b}}^{-1}\boldsymbol{S}_{\mathrm{b}}+\boldsymbol{S}_{\mathrm{s}}^{\mathrm{T}}\boldsymbol{D}_{\mathrm{s}}^{-1}\boldsymbol{S}_{\mathrm{s}})\mathrm{d}A \tag{13-104}$$

in which $\boldsymbol{D}_{\mathrm{b}}$ and $\boldsymbol{D}_{\mathrm{s}}$ are given by Eq. (12-49).

(3) The additional energy H_{pc} on the interface

The additional energy H_{pc} on the interface line S_{pc} of the two regions is (see Eq. (12-58)):

$$H_{\mathrm{pc}}=\int_{S_{\mathrm{pc}}}(Q_n\overline{w}+M_n\overline{\psi}_n+M_{ns}\overline{\psi}_s)\mathrm{d}s=\int_{S_{\mathrm{pc}}}\boldsymbol{T}^{\mathrm{T}}\overline{\boldsymbol{u}}\mathrm{d}s \tag{13-105}$$

where Q_n, M_n and M_{ns} are the three components of the boundary forces $\boldsymbol{T}$ of the C-region on the interface; $\overline{w}$, $\overline{\psi}_n$ and $\overline{\psi}_s$ are the three components of the boundary displacements $\overline{\boldsymbol{u}}$ of the P-region on the interface.

The boundary forces $\boldsymbol{T}$ can be expressed in terms of the stress parameters $\boldsymbol{\beta}$, and the boundary displacements $\overline{\boldsymbol{u}}$ can be expressed in terms of the nodal displacements $\overline{\boldsymbol{\delta}}$ on the interface. Since the C-region is a sectorial region, and the interface S_{pc} is a circular arc, the polar coordinates are used. Let

$$\left.\begin{aligned} \boldsymbol{T} &= [Q_r \quad M_r \quad M_{r\theta}]^{\mathrm{T}} = \boldsymbol{R}\boldsymbol{\beta} \\ \overline{\boldsymbol{u}} &= [\overline{w} \quad \overline{\psi}_r \quad \overline{\psi}_\theta]^{\mathrm{T}} = \boldsymbol{L}[\overline{w} \quad \overline{\psi}_x \quad \overline{\psi}_y]^{\mathrm{T}} = \boldsymbol{L}\overline{\boldsymbol{N}}\overline{\boldsymbol{\delta}} \end{aligned}\right\} \tag{13-106}$$

where $\boldsymbol{R}$ can be derived from the internal force fields around the notch-tip; $\boldsymbol{L}$ is a transformation matrix:

$$\boldsymbol{L} = \begin{bmatrix} 1 & 0 & 0 \\ 0 & \cos\theta & \sin\theta \\ 0 & -\sin\theta & \cos\theta \end{bmatrix} \tag{13-107}$$

$\overline{\boldsymbol{N}}$ is given by the shape functions of the 8-node isoparametric thick plate element

$$\overline{\boldsymbol{N}} = \left[\begin{array}{ccc:ccc:c:ccc} \overline{N}_1 & 0 & 0 & \overline{N}_2 & 0 & 0 & \cdots & \overline{N}_m & 0 & 0 \\ 0 & \overline{N}_1 & 0 & 0 & \overline{N}_2 & 0 & \cdots & 0 & \overline{N}_m & 0 \\ 0 & 0 & \overline{N}_1 & 0 & 0 & \overline{N}_2 & \cdots & 0 & 0 & \overline{N}_m \end{array}\right] \tag{13-108}$$

m is the number of the nodes on the interface. $\overline{\boldsymbol{\delta}}$ is the nodal displacement vector on the interface.

Substituting Eq. (13-106) into Eq. (13-105), the additional energy on the interface can be written in the form of Eq. (12-11):

$$H_{\text{pc}} = \boldsymbol{\beta}^{\mathrm{T}}\boldsymbol{H}\overline{\boldsymbol{\delta}} \tag{13-109}$$

where

$$\boldsymbol{H} = \int_{S_{\text{pc}}} \boldsymbol{R}^{\mathrm{T}}\boldsymbol{L}\overline{\boldsymbol{N}}\mathrm{d}s \tag{13-110}$$

(4) Solutions of the stress intensity factors

The energy functional Π above has already been expressed in terms of $\boldsymbol{\delta}$ and $\boldsymbol{\beta}$. From the stationary conditions, the fundamental Eqs. (12-19) and (12-16) can be derived. Then, $\boldsymbol{\delta}$ and $\boldsymbol{\beta}$ can be solved in turn, and the internal forces can also be obtained. Finally, we obtain

$$\left.\begin{aligned} K_{\mathrm{I}} &= \sqrt{2}\lim_{r\to 0} r^{1-\lambda_1} M_\theta\big|_{\theta=0} = -\sqrt{2}D\{(\mu-1)\lambda_1 + m_{01}[1+\lambda_1\mu - K_{01}(\lambda_1-1)]\}\beta_1 \\ K_{\mathrm{II}} &= \sqrt{2}\lim_{r\to 0} r^{1-\lambda_3} M_{r\theta}\big|_{\theta=0} = -\frac{\sqrt{2}}{2}D(1-\mu)[2\lambda_3 + m'_{03}(\lambda_3-1)(1+K_{03})]\beta_3 \\ K_{\mathrm{III}} &= \sqrt{2}\lim_{r\to 0} r^{1-\lambda_2} Q_\theta\big|_{\theta=0} = \sqrt{2}C\lambda_2\beta_2 \end{aligned}\right\} \tag{13-111}$$

The sub-region mixed element method for the V-notch problem in thick plate is denoted as SRM-V4.

Several numerical examples are given as follows.

Example 13.6 Stress intensity factor of mode Ⅰ for the V-notch problem in an infinite plate subjected to uniform bending moment.

An infinite rectangular plate with a rhombic hole is shown in Fig. 13.14. Its periphery is subjected to uniform bending moment *M*. The inner angle of the rhombic hole is α, and the length of diagonal line is $2a$.

In order to simulate the infinite plate, the side lengths of the rectangular plate are assumed as $2L = 2W = 20a$ during computation. And, $E = 2\times 10^6$, $\mu = 0.3$. Owing to symmetry, only 1/4 of the plate is used for computation. The division of the C-region and P-region is shown in Fig. 13.15. The C-region is a sector centered at the notch-tip, and its radius is r_c.

The 8-node isoparametric thick plate element is used for the P-region, and the mesh divisions are shown in Fig. 13.16(a),(b).

The results for the stress intensity factor K_{I}^{∞} (mode Ⅰ) with various opening angles are listed in Table 13.11. Along with the decrease of the opening angle α,

Table 13.11 $K_{\mathrm{I}}^{\infty}/M\sqrt{a}$ of an infinite plate with various opening angles of the notch

h/*a* \ $\alpha/2$	0°	15°	30°	45°	60°
1.0	0.7343	0.7899	0.8010	0.8515	0.9405
1.5	0.7874	0.8423	0.8540	0.8969	0.9890
2.0	0.8236	0.8917	0.8977	0.9305	1.0090

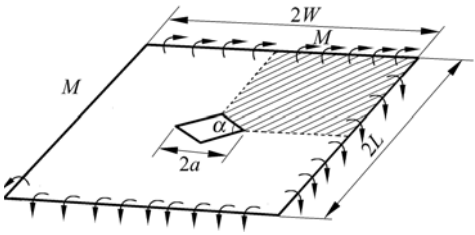

Figure 13.14 An infinite plate with V-notch subjected to uniform bending moment

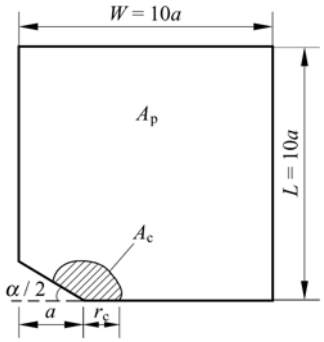

Figure 13.15 The division of the C-region and P-region (V-notch in thick plate)

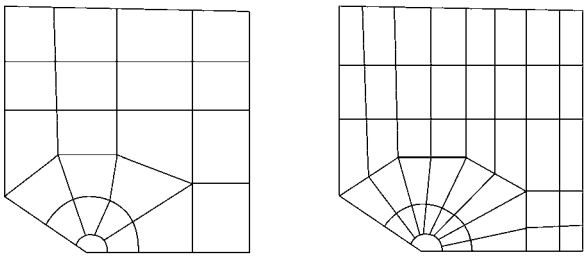

Figure 13.16 The mesh divisions of the P-region

the results will tend to be the analytical solutions of the crack problem[23], and errors are within 1%.

Example 13.7 The stress intensity factor K_1 of the V-notch in a finite plate.

The dimensions of the plate are $2L = 2W = 4a$, and the other data are the same as those in Example 13.6. The results for the stress intensity factor K_1 with various opening angles are listed in Table 13.12.

Table 13.12 K_1 of a finite plate with various opening angles of the notch

h/a \ $\alpha/2$	0°	15°	30°	45°	60°
1.0	0.8962	0.9418	0.9565	1.008	1.146
1.5	0.9901	1.045	1.058	1.115	1.250
2.0	1.055	1.112	1.118	1.162	1.288

In the above two examples, the radius of the C-region $r_c = 0.08a$. And, the highest order terms used here in the asymptotic solutions of the stresses at the notch-tip are r^{λ_2} (for M) and r^{λ_2+1} (for Q), respectively. It can be concluded that the computational results are basically stable.

13.6 3D V-Notch Problem

This section will discuss the 3D V-notch problem[4]. Firstly, by the expansion of the double power series, the eigenequaiton of the 3D V-notch problem is derived. Then, the eigenvalue series for notches with various inner opening angles are solved by the Muller iteration method, in which the minimum positive eigenvalue can be used to reflect the singularity of the notch-tip and the relation between this singularity and the inner angle of the notch. If the inner angle of the notch is equal to π, the problem will degenerate to be a semi-infinite space problem, in which no singularity exists; if the inner angle of the notch increases to be 2π, the problem will transfer to the 3D crack problem, in which the crack-tip possesses singularity with 1/2 order. For the general notch, the eigenvalue series can be decomposed into two parts, symmetric part and antisymmetric part. The corresponding displacement fields of the notch-tip are first derived; then the stress fields of the notch-tip are solved by the stress-displacement or strain-displacement relations.

13.6.1 The Differential Equations and Boundary Conditions for the 3D V-Notch Problem

As shown in Fig. 13.17, a 3D V-notch is considered. Its inner angle is α, and $\pi < \alpha < 2\pi$. The line of the notch-tip coincides with the z-axis, and can be infinitely extended forward and backward. The equations of the two surfaces of the notch are $\theta = \frac{\alpha}{2}$ and $\theta = -\frac{\alpha}{2}$, respectively.

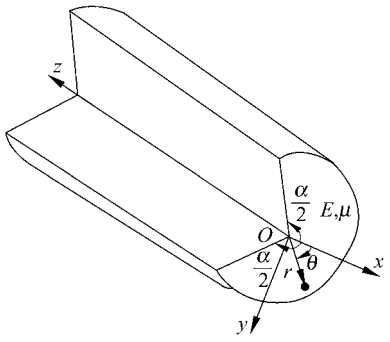

Figure 13.17 3D V-notch problem

By ignoring the influence of body forces and using the cylinder coordinate system, the equilibrium differential equations of this problem can be expressed in

terms of the stress components as follows:

$$\left.\begin{aligned}
&\frac{\partial \sigma_{rr}}{\partial r}+\frac{1}{r}\frac{\partial \sigma_{r\theta}}{\partial \theta}+\frac{\partial \sigma_{rz}}{\partial z}+\frac{1}{r}(\sigma_{rr}-\sigma_{\theta\theta})=0\\
&\frac{\partial \sigma_{r\theta}}{\partial r}+\frac{1}{r}\frac{\partial \sigma_{\theta\theta}}{\partial \theta}+\frac{\partial \sigma_{\theta z}}{\partial z}+\frac{2}{r}\sigma_{r\theta}=0\\
&\frac{\partial \sigma_{rz}}{\partial r}+\frac{1}{r}\frac{\partial \sigma_{\theta z}}{\partial \theta}+\frac{\partial \sigma_{zz}}{\partial z}+\frac{1}{r}\sigma_{rz}=0
\end{aligned}\right\} \tag{13-112}$$

The stress-displacement relations are

$$\left.\begin{aligned}
&\sigma_{rr}=\frac{E}{1+\mu}\left(\frac{\mu}{1-2\mu}e+\frac{\partial u_r}{\partial r}\right), \qquad \sigma_{\theta\theta}=\frac{E}{1+\mu}\left(\frac{\mu}{1-2\mu}e+\frac{1}{r}\frac{\partial u_\theta}{\partial \theta}+\frac{u_r}{r}\right)\\
&\sigma_{zz}=\frac{E}{1+\mu}\left(\frac{\mu}{1-2\mu}e+\frac{\partial u_z}{\partial z}\right), \qquad \sigma_{r\theta}=\frac{E}{2(1+\mu)}\left(\frac{\partial u_\theta}{\partial r}+\frac{1}{r}\frac{\partial u_r}{\partial \theta}-\frac{u_\theta}{r}\right)\\
&\sigma_{\theta z}=\frac{E}{2(1+\mu)}\left(\frac{1}{r}\frac{\partial u_z}{\partial \theta}+\frac{\partial u_\theta}{\partial z}\right), \qquad \sigma_{rz}=\frac{E}{2(1+\mu)}\left(\frac{\partial u_r}{\partial z}+\frac{\partial u_z}{\partial r}\right)
\end{aligned}\right\} \tag{13-113}$$

where E and μ are the Young's modulus and the Poisson's ratio of the material, respectively; and $e=\frac{\partial u_r}{\partial r}+\frac{1}{r}\frac{\partial u_\theta}{\partial \theta}+\frac{u_r}{r}+\frac{\partial u_z}{\partial z}$.

Substitution of Eq. (13-113) into Eq. (13-112) yields the equilibrium differential equations expressed by displacements:

$$\left.\begin{aligned}
&(X+G)\frac{\partial e}{\partial r}+G\nabla^2 u_r-G\frac{u_r}{r^2}-2G\frac{1}{r^2}\frac{\partial u_\theta}{\partial \theta}=0\\
&(X+G)\frac{1}{r}\frac{\partial e}{\partial \theta}+G\nabla^2 u_\theta+\frac{2G}{r^2}\frac{\partial u_r}{\partial \theta}-\frac{G}{r^2}u_\theta=0\\
&(X+G)\frac{\partial e}{\partial z}+G\nabla^2 u_z=0
\end{aligned}\right\} \tag{13-114}$$

where

$$X=\frac{E\mu}{(1+\mu)(1-2\mu)}, \quad G=\frac{E}{2(1+\mu)}, \quad \nabla^2=\frac{\partial^2}{\partial r^2}+\frac{1}{r}\frac{\partial}{\partial r}+\frac{1}{r^2}\frac{\partial^2}{\partial \theta^2}+\frac{\partial^2}{\partial z^2}$$

The boundary conditions of the notch (see Fig. 13.17) can be expressed by

$$\sigma_{\theta\theta}=\sigma_{\theta r}=\sigma_{\theta z}=0 \quad \left(\theta=\pm\frac{\alpha}{2}\right) \tag{13-115}$$

13.6.2 The Eigenequaiton and Eigenvalue of the 3D V-Notch Problem

The displacements u_r, u_θ and u_z can be expanded as the following double power series:

$$\left.\begin{aligned} u_r &= \sum_j \sum_n r^{\lambda_j+n} a_{nj}(\lambda_j,\theta,z) \\ u_\theta &= \sum_j \sum_n r^{\lambda_j+n} b_{nj}(\lambda_j,\theta,z) \\ u_z &= \sum_j \sum_n r^{\lambda_j+n} c_{nj}(\lambda_j,\theta,z) \end{aligned}\right\} \tag{13-116}$$

where $n = 0,1,2,\cdots$; $j = 1,2,\cdots$; and λ_1, λ_2, $\cdots$ are the eigenvalue series.

Substitution of Eq. (13-116) into Eq. (13-114) yields

$$\begin{aligned} &\sum_j \sum_n [\{(X+G)[((\lambda_j+n)^2-1)a_{nj} + (\lambda_j+n-1)b'_{nj}] + G[((\lambda_j+n)^2-1)a_{nj} \\ &\quad + a''_{nj} - 2b'_{nj}]\} r^{\lambda_j+n-2} + (X+G)(\lambda_j+n)c^{\cdot}_{nj} r^{\lambda_j+n-1} + Ga^{\cdot\cdot}_{nj} r^{\lambda_j+n}] = 0 \end{aligned} \tag{13-117a}$$

$$\begin{aligned} &\sum_j \sum_n [\{(X+G)[(\lambda_j+n+1)a'_{nj} + b''_{nj}] + G[2a'_{nj} + ((\lambda_j+n)^2-1)b_{nj} + b''_{nj}]\} r^{\lambda_j+n-2} \\ &\quad + (X+G)c'^{\cdot}_{nj} r^{\lambda_j+n-1} + Gb^{\cdot\cdot}_{nj} r^{\lambda_j+n}] = 0 \end{aligned} \tag{13-117b}$$

$$\begin{aligned} &\sum_j \sum_n [G[(\lambda_j+n)^2 c_{nj} + c''_{nj}] r^{\lambda_j+n-2} \\ &\quad + (X+G)[(\lambda_j+n+1)a^{\cdot}_{nj} + b'^{\cdot}_{nj}] r^{\lambda_j+n-1} + (X+2G)c^{\cdot\cdot}_{nj} r^{\lambda_j+n}] = 0 \end{aligned} \tag{13-117c}$$

where $\dfrac{\partial a}{\partial \theta}$ and $\dfrac{\partial a}{\partial z}$ are denoted by a' and $a^{\cdot}$, respectively. In the above equation set, by letting the sum of the coefficients of r terms with the same power order to be zero, equation set for each order will be obtained. The lowest order equation set (called the zero-order equation set) can be established by letting the sum of the coefficients of r^{λ_j-2} terms to be zero, i.e.,

$$\left.\begin{aligned} &(X+G)[(\lambda_j^2-1)a_{0j} + (\lambda_j-1)b'_{0j}] + G[(\lambda_j^2-1)a_{0j} + a''_{0j} - 2b'_{0j}] = 0 \\ &(X+G)[(\lambda_j+1)a'_{0j} + b''_{0j}] + G[2a'_{0j} + (\lambda_j^2-1)b_{0j} + b''_{0j}] = 0 \\ &\lambda_j^2 c_{0j} + c''_{0j} = 0 \end{aligned}\right\} \tag{13-118}$$

This is a homogenous ordinary differential equation set about a_{0j}, b_{0j} and c_{0j}.

Similarly, the first order equation set is obtained by letting the sum of the coefficients of r^{λ_j-1} terms in Eq. (13-117) be zero. This is a homogenous ordinary differential equation set about (a_{1j}, b_{1j}, c_{1j}) and (a_{0j}, b_{0j}, c_{0j}), from which a_{1j}, b_{1j} and c_{1j} can be solved.

According to the above procedure, equation set for each order can be derived in turn, and a_{nj}, b_{nj} and c_{nj} ($n=2,3,\cdots$) of each order can also be solved in turn.

The solution procedure for the zero-order equation set (13-118) (can be compared with that for Eq. (13-72)) will be discussed in detail as follows:

Firstly, the solutions of Eq. (13-118) can be expressed by

$$\left.\begin{aligned} a_{0j} &= A_{0j}\cos(\lambda_j+1)\theta + B_{0j}\sin(\lambda_j+1)\theta + D_{0j}\cos(\lambda_j-1)\theta + F_{0j}\sin(\lambda_j-1)\theta \\ b_{0j} &= B_{0j}\cos(\lambda_j+1)\theta - A_{0j}\sin(\lambda_j+1)\theta + K_{0j}[F_{0j}\cos(\lambda_j-1)\theta - D_{0j}\sin(\lambda_j-1)\theta] \\ c_{0j} &= P_{0j}\cos\lambda_j\theta + Q_{0j}\sin\lambda_j\theta \end{aligned}\right\} \tag{13-119}$$

in which A_{0j}, B_{0j}, D_{0j}, F_{0j}, P_{0j} and Q_{0j} are the undetermined coefficients and functions of z; and $K_{0j}=\dfrac{\lambda_j+3-4\mu}{\lambda_j-3+4\mu}$.

Secondly, the corresponding boundary conditions are introduced. Substitution of Eq. (13-116) into the boundary conditions (13-115) yields the following zero-order boundary conditions

$$\left.\begin{aligned} &b'_{0j}+\left(1+\frac{\mu\lambda_j}{1-\mu}\right)a_{0j}=0 \\ &a'_{0j}+(\lambda_j-1)b_{0j}=0 \\ &c'_{0j}=0 \end{aligned}\right\} \quad \left(\theta=\pm\frac{\alpha}{2}\right) \tag{13-120}$$

Substituting Eq. (13-119) into the above equation, the following 6 conditions can be obtained:

$$\frac{2\mu-1}{1-\mu}\lambda_j A_{0j}\cos(\lambda_j+1)\frac{\alpha}{2}+\left[-K_{0j}(\lambda_j-1)+1+\frac{\lambda_j\mu}{1-\mu}\right]D_{0j}\cos(\lambda_j-1)\frac{\alpha}{2}=0 \tag{13-121a}$$

$$2A_{0j}\lambda_j\sin(\lambda_j+1)\frac{\alpha}{2}-(\lambda_j-1)(1+K_{0j})D_{0j}\sin(\lambda_j-1)\frac{\alpha}{2}=0 \tag{13-121b}$$

$$\frac{2\mu-1}{1-\mu}\lambda_j B_{0j}\sin(\lambda_j+1)\frac{\alpha}{2}+\left[-K_{0j}(\lambda_j-1)+1+\frac{\lambda_j\mu}{1-\mu}\right]F_{0j}\sin(\lambda_j-1)\frac{\alpha}{2}=0 \tag{13-121c}$$

$$2B_{0j}\lambda_j \cos(\lambda_j+1)\frac{\alpha}{2}+(\lambda_j-1)(1+K_{0j})F_{0j}\cos(\lambda_j-1)\frac{\alpha}{2}=0 \tag{13-121d}$$

$$Q_{0j}\lambda_j \cos\lambda_j\frac{\alpha}{2}=0 \tag{13-121e}$$

$$P_{0j}\lambda_j \sin\lambda_j\frac{\alpha}{2}=0 \tag{13-121f}$$

This is a homogenous equation set about A_{0j}, B_{0j}, D_{0j}, F_{0j}, Q_{0j} and P_{0j}. If this homogenous equation set has nontrivial solutions, its determinant of coefficients should be equal to zero, i.e.,

$$(\sin\lambda_j\alpha+\lambda_j\sin\alpha)(\sin\lambda_j\alpha-\lambda_j\sin\alpha)\sin\frac{\lambda_j\alpha}{2}\cos\frac{\lambda_j\alpha}{2}=0 \tag{13-122}$$

This is the eigenequation for the 3D V-notch problem, which is completely the same as the eigenequation (13-76) for the V-notch problem in the Reissner plate. Therefore, the eigenvalues of the V-notch problem in the Reissner plate listed in Table 13.10 are still suitable for the 3D V-notch problem.

It can be recalled that, the eigenequation (13-122) can be decomposed into the following four equations (i.e. Eq. (13-77)):

$$\sin\lambda_j\alpha+\lambda_j\sin\alpha=0 \tag{13-123a}$$

$$\sin\lambda_j\alpha-\lambda_j\sin\alpha=0 \tag{13-123b}$$

$$\cos\lambda_j\frac{\alpha}{2}=0 \tag{13-123c}$$

$$\sin\lambda_j\frac{\alpha}{2}=0 \tag{13-123d}$$

which are corresponding to the following four cases:

A_{0j} and D_{0j} in Eqs. (13-121a,b) have nontrivial solutions—symmetric state;

B_{0j} and F_{0j} in Eqs. (13-121 c,d) have nontrivial solutions—antisymmetric state;

Q_{0j} in Eq. (13-121e) has nontrivial solution—antisymmetric state;

P_{0j} in Eq. (13-121f) has nontrivial solution—symmetric state.

Load states in the 3D V-notch problem can be classified as symmetric state and antisymmetric state. And, the eigenvalue series $\boldsymbol{\lambda}$ can also be classified as two sub series of symmetry and antisymmetry:

Symmetric sub series $\{\lambda_1,\lambda_4,\lambda_5,\lambda_8,\cdots\}$—the combination of the eigenvalues of Eqs. (13-123a,d).

Antisymmetric sub series $\{\lambda_2,\lambda_3,\lambda_6,\lambda_7,\cdots\}$—the combination of the eigenvalues of Eqs. (13-123b,c).

The following discussions on the displacement and stress fields around notch-tip are also classified as two cases of symmetry and antisymmetry.

13.6.3 Stress Fields Around 3D Notch-Tip—the Symmetric State

The symmetric sub series of eigenvalues can be divided into two groups

$$\text{Group a:} \quad [\lambda_1, \lambda_5, \lambda_9, \cdots]$$

$$\text{Group b:} \quad [\lambda_4, \lambda_8, \lambda_{12}, \cdots]$$

Here, the results of the first two orders ($n = 0$ and $n = 1$) are given as follows.

(1a) $n = 0, j = 1,5,9, \cdots$

Eigenvalue λ_j of this group satisfies Eq. (13-123a). Substitution of it into Eq. (13-121b) or Eq. (13-121a) yields

$$A_{0j} = m_{0j} D_{0j}$$

where

$$m_{0j} = \frac{(\lambda_j - 1)(1 + K_{0j})}{2\lambda_j} \frac{\sin\frac{1}{2}(\lambda_j - 1)\alpha}{\sin\frac{1}{2}(\lambda_j + 1)\alpha}$$

Then, from Eq. (13-121c) to Eq. (13-121f), we have

$$B_{0j} = F_{0j} = Q_{0j} = P_{0j} = 0$$

Substituting them into Eqs. (13-119) and (13-116), the corresponding displacement terms can be derived:

$$\left.\begin{aligned} u_r &= r^{\lambda_j}[m_{0j}\cos(\lambda_j + 1)\theta + \cos(\lambda_j - 1)\theta]\beta_j \\ u_\theta &= -r^{\lambda_j}[m_{0j}\sin(\lambda_j + 1)\theta + K_{0j}\sin(\lambda_j - 1)\theta]\beta_j \\ u_z &= 0 \end{aligned}\right\} \tag{13-124}$$

in which β_j is just D_{0j}, it is a function of z ($j = 1,5,9, \cdots$). By the stress-displacement relation (13-113), the corresponding stress field can be obtained:

$$\left.\begin{aligned} \sigma_{rr} &= r^{\lambda_j - 1}\{[X(\lambda_j - 1) - XK_{0j}(\lambda_j - 1) + 2G\lambda_j]\cos(\lambda_j - 1)\theta + 2G\lambda_j m_{0j}\cos(\lambda_j + 1)\theta\}\beta_j \\ \sigma_{\theta\theta} &= r^{\lambda_j - 1}\{[X(\lambda_j + 1) - XK_{0j}(\lambda_j - 1) + 2G \\ &\quad - 2GK_{0j}(\lambda_j - 1)]\cos(\lambda_j - 1)\theta - 2G\lambda_j m_{0j}\cos(\lambda_j + 1)\theta\}\beta_j \\ \sigma_{zz} &= r^{\lambda_j - 1}\{[X(\lambda_j + 1) - K_{0j}(\lambda_j - 1)]\cos(\lambda_j - 1)\theta\}\beta_j \\ \sigma_{r\theta} &= r^{\lambda_j - 1}G[-2m_{0j}\lambda_j\sin(\lambda_j + 1)\theta - (\lambda_j - 1)(1 + K_{0j})\sin(\lambda_j - 1)\theta]\beta_j \\ \sigma_{\theta z} &= r^{\lambda_j}G[-m_{0j}\sin(\lambda_j + 1)\theta - K_{0j}\sin(\lambda_j - 1)\theta]\beta_j \\ \sigma_{rz} &= r^{\lambda_j}G[m_{0j}\cos(\lambda_j + 1)\theta + \cos(\lambda_j - 1)\theta]\beta_j \end{aligned}\right\} \tag{13-125}$$

(1b) $n=0, j=4,8,12,\cdots$

The eigenvalue λ_j of this group satisfies Eq. (13-123d). Substitution of it into Eq. (13-121f) yields

$$P_{0j} \neq 0$$

And, from the other expressions in Eq. (13-121), we obtain

$$A_{0j} = D_{0j} = B_{0j} = F_{0j} = Q_{0j} = 0$$

Substituting them into Eqs. (13-119) and (13-116), the corresponding displacement terms can be obtained

$$u_r = 0, \quad u_\theta = 0, \quad u_z = r^{\lambda_j}\beta_j \cos\lambda_j\theta \tag{13-126}$$

in which β_j is just P_{0j} ($j=4,8,12,\cdots$).

The corresponding stress terms can be solved from Eq. (13-113) as follows:

$$\left.\begin{aligned} &\sigma_{rr} = r^{\lambda_j} X\beta_j^{\cdot} \cos\lambda_j\theta, && \sigma_{\theta\theta} = r^{\lambda_j} X\beta_j^{\cdot} \cos\lambda_j\theta \\ &\sigma_{zz} = r^{\lambda_j}(2G+X)\beta_j^{\cdot} \cos\lambda_j\theta, && \sigma_{r\theta} = 0 \\ &\sigma_{\theta z} = -r^{\lambda_j-1} G\lambda_j\beta_j \sin\lambda_j\theta, && \sigma_{rz} = r^{\lambda_j-1} G\lambda_j\beta_j \cos\lambda_j\theta \end{aligned}\right\} \tag{13-127}$$

(2a) $n=1$， $j=1,5,9,\cdots$

The case of $n=1$ is corresponding to the first-order equation set and the first-order displacement and stress terms. By letting the sum of the coefficients of r^{λ_j-1} terms in Eq. (13-117) be zero, an ordinary differential equation set about (a_{1j}, b_{1j}, c_{1j}) and (a_{0j}, b_{0j}, c_{0j}) can be obtained as follows:

$$\left.\begin{aligned} &(X+G)\{[(\lambda_j+1)^2-1]a_{1j} + \lambda_j b'_{1j}\} \\ &\quad + G\{[(\lambda_j+1)^2-1]a_{1j} + a''_{1j} - 2b'_{1j}\} + (X+G)\lambda_j c^{\cdot}_{0j} = 0 \\ &(X+G)[(\lambda_j+2)a'_{1j} + b''_{1j}] + G\{2a'_{1j} + [(\lambda_j+1)^2-1]b'_{1j} + b''_{1j}\} + (X+G)c'^{\cdot}_{0j} = 0 \\ &G[(\lambda_j+1)^2 c_{1j} + c''_{1j}] + (X+G)[(\lambda_j+1)a^{\cdot}_{0j} + b'^{\cdot}_{0j}] = 0 \end{aligned}\right\} \tag{13-128}$$

When $j=1,5,9,\cdots$, (a_{0j}, b_{0j}, c_{0j}) in the above equation can be obtained from Eq. (13-124):

$$\left.\begin{aligned} a_{0j} &= [m_{0j}\cos(\lambda_j+1)\theta + \cos(\lambda_j-1)\theta]\beta_j \\ b_{0j} &= -[m_{0j}\sin(\lambda_j+1)\theta + K_{0j}\sin(\lambda_j-1)\theta]\beta_j \\ c_{0j} &= 0 \end{aligned}\right\} \tag{13-129}$$

Substituting the above equation into Eq. (13-128), (a_{1j}, b_{1j}, c_{1j}) can be solved as follows:

$$\left.\begin{aligned} a_{1j} &= A_{1j}\cos(\lambda_j+2)\theta + B_{1j}\sin(\lambda_j+2)\theta + D_{1j}\cos\lambda_j\theta + F_{1j}\sin\lambda_j\theta \\ b_{1j} &= B_{1j}\cos(\lambda_j+2)\theta - A_{1j}\sin(\lambda_j+2)\theta + K_{1j}[F_{1j}\cos\lambda_j\theta - D_{1j}\sin\lambda_j\theta] \\ c_{1j} &= P_{1j}\cos(\lambda_j+1)\theta + Q_{1j}\sin(\lambda_j+1)\theta - \frac{X+G}{4\lambda_j G}[\lambda_j+1-K_{0j}(\lambda_j-1)]\beta_j^{\cdot}\cos(\lambda_j-1)\theta \end{aligned}\right\} \tag{13-130}$$

where

$$K_{1j} = -\frac{\lambda_j+1+3-4\mu}{\lambda_j+1-3+4\mu}$$

From the boundary condition (13-115), the first-order boundary conditions can be written by

$$\left.\begin{aligned} &b'_{1j} + \frac{\lambda_j\mu+1}{1-\mu}a_{1j} = 0 \\ &a'_{1j} + \lambda_j b_{1j} = 0 \\ &c'_{1j} - [m_{0j}\sin(\lambda_j+1)\theta + K_{0j}\sin(\lambda_j-1)\theta]\beta_j^{\cdot} = 0 \end{aligned}\right\} \quad \left(\theta = \pm\frac{\alpha}{2}\right) \tag{13-131}$$

Substitution of Eq. (13-130) into the above equation, we have

$$A_{1j} = B_{1j} = D_{1j} = F_{1j} = Q_{1j} = 0$$
$$P_{1j} = f_{1j}\beta_j^{\cdot}$$

where

$$f_{1j} = \frac{X+G}{4\lambda_j G}[(\lambda_j+1) - K_{0j}(\lambda_j-1)]\frac{\lambda_j-1}{\lambda_j+1}\frac{\sin\frac{1}{2}(\lambda_j-1)\alpha}{\sin\frac{1}{2}(\lambda_j+1)\alpha}$$
$$-\frac{m_{0j}\sin\frac{1}{2}(\lambda_j+1)\alpha + K_{0j}\sin\frac{1}{2}(\lambda_j-1)\alpha}{(\lambda_j+1)\sin\frac{1}{2}(\lambda_j+1)\alpha}$$

The corresponding displacement terms can be solved as follows

$$\left.\begin{aligned} u_r &= 0 \\ u_\theta &= 0 \\ u_z &= r^{\lambda_j+1}[f_{1j}\cos(\lambda_j+1)\theta + g_{1j}\cos(\lambda_j-1)\theta]\beta_j^{\cdot} \end{aligned}\right\} \tag{13-132}$$

where

$$g_{1j} = -\frac{X+G}{4\lambda_j G}[\lambda_j + 1 - K_{0j}(\lambda_j - 1)]$$

And, the corresponding stress terms are

$$\left.\begin{aligned}
\sigma_{rr} &= r^{\lambda_j+1} X[f_{1j}\cos(\lambda_j+1)\theta + g_{1j}\cos(\lambda_j-1)\theta]\beta_j^{\cdot\cdot} \\
\sigma_{\theta\theta} &= r^{\lambda_j+1} X[f_{1j}\cos(\lambda_j+1)\theta + g_{1j}\cos(\lambda_j-1)\theta]\beta_j^{\cdot\cdot} \\
\sigma_{zz} &= r^{\lambda_j+1}(X+2G)[f_{1j}\cos(\lambda_j+1)\theta + g_{1j}\cos(\lambda_j-1)\theta]\beta_j^{\cdot\cdot} \\
\sigma_{r\theta} &= 0 \\
\sigma_{\theta z} &= r^{\lambda_j} G[(\lambda_j+1)f_{1j}\sin(\lambda_j+1)\theta + (\lambda_j-1)g_{1j}\sin(\lambda_j-1)\theta]\beta_j^{\cdot} \\
\sigma_{rz} &= r^{\lambda_j} G\lambda_j[f_{1j}\cos(\lambda_j+1)\theta + g_{1j}\cos(\lambda_j-1)\theta]\beta_j^{\cdot}
\end{aligned}\right\} \quad (13\text{-}133)$$

(2b) $n=1, j=4,8,12,\cdots$

Now, the cases of $j=4,8,12,\cdots$ are considered. Here, a_{0j}, b_{0j} and c_{0j} can be obtained from Eq. (13-126):

$$a_{0j}=0, \quad b_{0j}=0, \quad c_{0j}=\beta_j\cos\lambda_j\theta \quad (13\text{-}134)$$

Substituting the above equation back into Eq. (13-128), a_{1j}, b_{1j} and c_{1j} can be solved as follows:

$$\left.\begin{aligned}
a_{1j} &= A_{1j}\cos(\lambda_j+2)\theta + B_{1j}\sin(\lambda_j+2)\theta + D_{1j}\cos\lambda_j\theta + F_{1j}\sin\lambda_j\theta \\
&\quad -\frac{X+G}{(X+G)(\lambda_j+2)+2G}\beta_j^{\cdot}\cos\lambda_j\theta \\
b_{1j} &= B_{1j}\cos(\lambda_j+2)\theta - A_{1j}\sin(\lambda_j+2)\theta + K_{1j}(F_{1j}\cos\lambda_j\theta - D_{1j}\sin\lambda_j\theta) \\
c_{1j} &= P_{1j}\cos(\lambda_j+1)\theta + Q_{1j}\sin(\lambda_j+1)\theta
\end{aligned}\right\} \quad (13\text{-}135)$$

From the boundary condition (13-115), the corresponding first-order boundary condition can be written as:

$$\left.\begin{aligned}
b_{1j}' + \frac{\lambda_j\mu+1}{1-\mu}a_{1j} + \frac{\mu}{1-\mu}\beta_j^{\cdot}\cos\lambda_j\theta &= 0 \\
a_{1j}' + \lambda_j b_{1j} &= 0 \\
c_{1j}' &= 0
\end{aligned}\right\} \quad \left(\theta = \pm\frac{\alpha}{2}\right) \quad (13\text{-}136)$$

Substitution of Eq. (13-135) into the above equation yields

$$\left.\begin{aligned} &B_{1j} = F_{1j} = Q_{1j} = P_{1j} = 0 \\ &A_{1j} = l_{1j}\beta_j^{\cdot},\quad D_{1j} = \gamma_{1j}\beta_j^{\cdot} \end{aligned}\right\} \tag{13-137}$$

where l_{1j} and γ_{1j} are given in Appendix C. The corresponding displacement terms are

$$\left.\begin{aligned} u_r &= r^{\lambda_j+1}[l_{1j}\cos(\lambda_j+2)\theta + h_{1j}\cos\lambda_j\theta]\beta_j^{\cdot} \\ u_\theta &= -r^{\lambda_j+1}[l_{1j}\sin(\lambda_j+2)\theta + K_{1j}\gamma_{1j}\sin\lambda_j\theta]\beta_j^{\cdot} \\ u_z &= 0 \end{aligned}\right\} \tag{13-138}$$

where

$$h_{1j} = \gamma_{1j} - \frac{X+G}{(X+G)(\lambda_j+2)+2G}$$

And, the corresponding stress terms are

$$\left.\begin{aligned} \sigma_{rr} &= r^{\lambda_j}\{[-XK_{1j}\gamma_{1j}\lambda_j + X(\lambda_j+2)g_{1j} + 2G\lambda_j g_{1j}]\cos\lambda_j\theta + 2G\lambda_j l_{1j}\cos(\lambda_j+2)\theta\}\beta_j^{\cdot} \\ \sigma_{\theta\theta} &= r^{\lambda_j}\{[-XK_{1j}\gamma_{1j}\lambda_j + X(\lambda_j+2)g_{1j} \\ &\quad + 2G(g_{1j} - K_{1j}\gamma_{1j}\lambda_j)]\cos\lambda_j\theta - 2Gl_{1j}(\lambda_j+1)\cos(\lambda_j+2)\theta\}\beta_j^{\cdot} \\ \sigma_{zz} &= r^{\lambda_j}\{X[-K_{1j}\gamma_{1j}\lambda_j + (\lambda_j+2)g_{1j}]\cos\lambda_j\theta\}\beta_j^{\cdot} \\ \sigma_{r\theta} &= -r^{\lambda_j}G[2l_{1j}(\lambda_j+1)\sin(\lambda_j+2)\theta + (g_{1j} + K_{1j}\gamma_{1j})\lambda_j\sin\lambda_j\theta]\beta_j^{\cdot} \\ \sigma_{\theta z} &= -r^{\lambda_j+1}G[l_{1j}\sin(\lambda_j+2)\theta + K_{1j}\gamma_{1j}\sin\lambda_j\theta]\beta_j^{\cdot\cdot} \\ \sigma_{rz} &= r^{\lambda_j+1}G[l_{1j}\cos(\lambda_j+2)\theta + g_{1j}\cos\lambda_j\theta]\beta_j^{\cdot\cdot} \end{aligned}\right\} \tag{13-139}$$

13.6.4 Stress Fields Around 3D Notch-Tip—the Antisymmetric State

The antisymmetric sub series of eigenvalues can be divided into two groups

$$\text{Group a:} \quad [\lambda_2, \lambda_6, \lambda_{10}, \cdots]$$

$$\text{Group b:} \quad [\lambda_3, \lambda_7, \lambda_{11}, \cdots]$$

Here, the results of the first two orders ($n = 0$ and $n = 1$) are given as follows.

(1a) $n = 0, j = 2,6,10,\cdots$

The displacement terms are

$$u_r = 0,\quad u_\theta = 0,\quad u_z = r^{\lambda_j}\beta_j\sin\lambda_j\theta \tag{13-140}$$

And, the stress terms are:

$$\left.\begin{aligned}
\sigma_{rr} &= r^{\lambda_j} X \beta_j^{\cdot} \sin\lambda_j\theta \\
\sigma_{\theta\theta} &= r^{\lambda_j} X \beta_j^{\cdot} \sin\lambda_j\theta \\
\sigma_{zz} &= r^{\lambda_j} (X+2G) \beta_j^{\cdot} \sin\lambda_j\theta \\
\sigma_{r\theta} &= 0 \\
\sigma_{\theta z} &= r^{\lambda_j - 1} G\lambda_j \beta_j \cos\lambda_j\theta \\
\sigma_{rz} &= r^{\lambda_j - 1} G\lambda_j \beta_j \sin\lambda_j\theta
\end{aligned}\right\} \tag{13-141}$$

(1b) $n=0, j=3,7,11,\cdots$
The displacement terms are

$$\left.\begin{aligned}
u_r &= r^{\lambda_j}[n_{0j}\sin(\lambda_j+1)\theta + \sin(\lambda_j-1)\theta]\beta_j \\
u_\theta &= r^{\lambda_j}[n_{0j}\cos(\lambda_j+1)\theta + K_{0j}\cos(\lambda_j-1)\theta]\beta_j \\
u_z &= 0
\end{aligned}\right\} \tag{13-142}$$

And, the stress terms are

$$\left.\begin{aligned}
\sigma_{rr} &= r^{\lambda_j-1}\{[X(\lambda_j+1) - XK_{0j}(\lambda_j-1) + 2G\lambda_j]\sin(\lambda_j-1)\theta \\
&\quad + 2Gn_{0j}\lambda_j \sin(\lambda_j+1)\theta\}\beta_j \\
\sigma_{\theta\theta} &= r^{\lambda_j-1}\{[X(\lambda_j+1) - XK_{0j}(\lambda_j-1) + 2G \\
&\quad - 2GK_{0j}(\lambda_j-1)]\sin(\lambda_j-1)\theta - 2Gn_{0j}\lambda_j\sin(\lambda_j+1)\theta\}\beta_j \\
\sigma_{zz} &= r^{\lambda_j-1} X\{[\lambda_j + 1 - K_{0j}(\lambda_j-1)]\sin(\lambda_j-1)\theta\}\beta_j \\
\sigma_{r\theta} &= r^{\lambda_j-1} G[2n_{0j}\lambda_j\cos(\lambda_j+1)\theta + (\lambda_j-1)(1+K_{0j})\cos(\lambda_j-1)\theta]\beta_j \\
\sigma_{\theta z} &= r^{\lambda_j} G[n_{0j}\cos(\lambda_j+1)\theta + K_{0j}\cos(\lambda_j-1)\theta]\beta_j^{\cdot} \\
\sigma_{rz} &= r^{\lambda_j} G[n_{0j}\sin(\lambda_j+1)\theta + \sin(\lambda_j-1)\theta]\beta_j^{\cdot}
\end{aligned}\right\} \tag{13-143}$$

where

$$n_{0j} = -\frac{(\lambda_j-1)(1+K_{0j})\cos\dfrac{1}{2}(\lambda_j-1)\alpha}{2\lambda_j\cos\dfrac{1}{2}(\lambda_j+1)\alpha}$$

(2a) $n=1, j=2,6,10,\cdots$

The displacement terms are

$$\left.\begin{aligned} u_r &= r^{\lambda_j+1}[s_{1j}\sin(\lambda_j+2)\theta + p_{1j}\sin\lambda_j\theta]\beta_j^{\cdot} \\ u_\theta &= r^{\lambda_j+1}[s_{1j}\cos(\lambda_j+2)\theta + K_{1j}t_{1j}\cos\lambda_j\theta]\beta_j^{\cdot} \\ u_z &= 0 \end{aligned}\right\} \tag{13-144}$$

where s_{1j} and t_{1j} are given in Appendix D,

$$p_{1j} = t_{1j} - \frac{X+G}{(X+G)(\lambda_j+2)+2G}$$

And, the stress terms are

$$\left.\begin{aligned} \sigma_{rr} &= r^{\lambda_j}\{[X(\lambda_j+2)\nu_{1j} - XK_{1j}\gamma_{1j}\lambda_j + 2G\lambda_j\nu_{1j}]\sin\lambda_j\theta + 2G\lambda_j s_{1j}\sin(\lambda_j+2)\theta\}\beta_j^{\cdot} \\ \sigma_{\theta\theta} &= r^{\lambda_j}\{[X(\lambda_j+2)\nu_{1j} - XK_{1j}\gamma_{1j}\lambda_j + 2G(\nu_{1j} - K_{1j}t_{1j}\lambda_j)]\sin\lambda_j\theta \\ &\quad - 2G(\lambda_j+1)s_{1j}\sin(\lambda_j+2)\theta\}\beta_j^{\cdot} \\ \sigma_{zz} &= r^{\lambda_j}X\{[(\lambda_j+2)\nu_{1j} - K_{1j}t_{1j}\lambda_j]\sin\lambda_j\theta\}\beta_j^{\cdot} \\ \sigma_{r\theta} &= r^{\lambda_j}G\{2(\lambda_j+1)s_{1j}\cos(\lambda_j+2)\theta + [\nu_{1j}\lambda_j + K_{1j}\lambda_j t_{1j}]\cos\lambda_j\theta\}\beta_j^{\cdot} \\ \sigma_{\theta z} &= r^{\lambda_j+1}G[s_{1j}\sin(\lambda_j+2)\theta + K_{1j}t_{1j}\cos\lambda_j\theta]\beta_j^{\cdot\cdot} \\ \sigma_{rz} &= r^{\lambda_j+1}G[s_{1j}\sin(\lambda_j+2)\theta + \nu_{1j}\cos\lambda_j\theta]\beta_j^{\cdot\cdot} \end{aligned}\right\} \tag{13-145}$$

(2b) $n = 1, j = 3,7,11,\cdots$

The displacement terms are

$$u_r = 0, \quad u_\theta = 0, \quad u_z = r^{\lambda_j}[q_{1j}\sin(\lambda_j+1)\theta + \nu_{1j}\sin(\lambda_j-1)\theta]\beta_j^{\cdot} \tag{13-146}$$

where

$$q_{1j} = \frac{X+G}{4\lambda_j G}[(\lambda_j+1) - K_{0j}(\lambda_j-1)]\frac{\lambda_j-1}{\lambda_j+1}\frac{\cos\frac{1}{2}(\lambda_j-1)\alpha}{\cos\frac{1}{2}(\lambda_j+1)\alpha}$$

$$-\frac{n_{0j}\cos\frac{1}{2}(\lambda_j+1)\alpha + K_{0j}\cos\frac{1}{2}(\lambda_j-1)\alpha}{(\lambda_j+1)\cos\frac{1}{2}(\lambda_j+1)\alpha}$$

$$\nu_{1j} = -\frac{X+G}{4\lambda_j G}[\lambda_j + 1 - K_{0j}(\lambda_j-1)]$$

And, the stress terms are

$$\left.\begin{aligned}
\sigma_{rr} &= r^{\lambda_j+1}X[q_{1j}\sin(\lambda_j+1)\theta + v_{1j}\sin(\lambda_j-1)\theta]\beta_j^{\cdot\cdot} \\
\sigma_{\theta\theta} &= r^{\lambda_j+1}X[q_{1j}\sin(\lambda_j+1)\theta + v_{1j}\sin(\lambda_j-1)\theta]\beta_j^{\cdot\cdot} \\
\sigma_{zz} &= r^{\lambda_j+1}(X+2G)[q_{1j}\sin(\lambda_j+1)\theta + v_{1j}\sin(\lambda_j-1)\theta]\beta_j^{\cdot\cdot} \\
\sigma_{r\theta} &= 0 \\
\sigma_{\theta z} &= r^{\lambda_j}G[(\lambda_j+1)q_{1j}\cos(\lambda_j+1)\theta + (\lambda_j-1)v_{1j}\cos(\lambda_j-1)\theta]\beta_j^{\cdot} \\
\sigma_{rz} &= r^{\lambda_j}G\lambda_j[q_{1j}\sin(\lambda_j+1)\theta + v_{1j}\sin(\lambda_j-1)\theta]\beta_j^{\cdot}
\end{aligned}\right\} \quad (13\text{-}147)$$

When the inner angle tends to be 2π, the above solutions can be transferred to the displacement and stress fields of a crack in 3D space, which are identical with the results given by reference [24].

The sub-region mixed element method for the 3D V-notch problem is denoted by SRM-V5.

References

[1] Fan Z, Long YQ (1992) Sub-region mixed finite element analysis of V-notched plates. International Journal of Fracture 56: 333 – 344

[2] Long YQ, Qian J (1992) Sub-region mixed finite element analysis of V-notches in a bimaterial. In: Zhu DC (ed) Advances in Engineering Mechanics, Peking University Press, Beijing, pp54 – 59

[3] Qian J, Long YQ (1992) The expression of stress and strain at the tip of notch in Reissner plate. Applied mathematics and Mechanics (English Edition) 13(4): 315 – 324

[4] Qian J, Long YQ (1994) The expression of stress and strain at the tip of 3-D notch. Applied mathematics and Mechanics (English Edition) 15(3): 211 – 221

[5] Williams ML (1952) Stress singularities resulting from various boundary conditions in angular corners of plates in extension. Journal of Applied Mechanics 14: 526 – 528

[6] Gross B, Mendelson A (1972) Plane elastostatic analysis of V-notched plates. International Journal of Fracture 8: 267 – 276

[7] Rzasnicki W, Mendelson A, Albers LU (1973) Application of boundary integral method to elastic analysis of V-notched beams. NASA TN-F-7424

[8] Carpenter WC (1984) A collocation procedure for determining fracture mechanics parameters at a corner. International Journal of Fracture 24: 255 – 266

[9] Carpenter WC (1985) The eigenvector solution for a general corner or finite opening crack with further studies on the collocation procedure. International Journal of Fracture 27: 63 – 74

[10] Carpenter WC (1987) A path independent integral for computing stress intensities for V-notched cracks in a bi-material. International Journal of Fracture 35: 245 – 268

[11] Lin KY, Tong P (1980) Singular finite element for the fracture analysis of V-notch plate. International Journal for Numerical Methods in Engineering 15: 1343 – 1354
[12] Awaji H, Yokobori AT, Yokobori T (1986) The variation of the stress singularity at the notch-tip as notch angle and radius of curvature. Computers & Structures 22(1): 25 – 30
[13] Long YQ (1987) Variational Principles •Finite Element Method •Shell Analysis. Liaoning Science and Technology Publishing House, Shenyang (in Chinese)
[14] Lin KY, Mar JW (1976) Finite element analysis of stress intensity factors for cracks at a bi-material interface. International Journal of Fracture 12: 521 – 531
[15] Rice JR, Sih GC (1965) Plane problems of cracks in dissimilar media. Journal of Applied Mechanics 32: 418 – 423
[16] Qian J, Long YQ (1991) Sub region mixed FEM for calculating stress intensity factor of antiplane notch in bi-material. Computational Structural Mechanics and Applications 8(3): 325 – 330 (in Chinese)
[17] Sham TL, Bueckner HF (1988) The weight function theory for piecewise homogeneous isotropic notches in antiplane strain. Journal of Applied Mechanics 55: 956 – 603
[18] Sham TL (1988) Weight functions for piecewise homogeneous isotropic notches in antiplane strain by finite element method. Engineering Fracture Mechanics 31(4): 567 – 576
[19] Schovanec L (1989) An antiplane shear crack in a nonhomogeneous elastic material. Engineering Fracture Mechanics 33: 745 – 751
[20] Hwang KC, Yu SW (1985) Fracture mechanics in elasticity and plasticity. Tsinghua University Press, Beijing (in Chinese)
[21] Liu CT (1983) Stresses and deformations near the crack tip for bending plate. Acta Mechanica Solida Sinica 3: 441 – 448 (in Chinese)
[22] Knowles JK, Wang NM (1960) On the bending of an elastic plate containing a crack. Journal of Mathematics and Physics 39: 223 – 236
[23] Hartanft RJ, Sih GC (1968) Effect of plate thickness on the bending stress distribution around through cracks. Journal of Mathematics and Physics 47: 276 – 291
[24] Hartranft RJ, Sih GC (1969) The use of eigenfunction expansions in the general solution of three dimensional crack problems. Journal of Mathematics and Mechanics 19: 123 – 138